https://doi.org/10.5194/egusphere-2026-4273
Preprint. Discussion started: 31 July 2026

A Predictability Pathway from Franklin to Daniel: Linking Extratropical Transition, European Blocking, and Devastating Mediterranean Cyclone Daniel

Jake P. Keller[1], Oscar Martínez-Alvarado[1, 2], Ben J. Harvey[1, 2], Claudio Sanchez[3], and Benoît Vannière[4]

[1]Department of Meteorology, Brian Hoskins Building, Whiteknights Road, Earley Gate, University of Reading, Reading, RG6 6ET, UK
[2]National Centre for Atmospheric Science, University of Reading, Earley Gate, Reading, RG6 6BB, UK
[3]Met Office, FitzRoy Road, Exeter, Devon, EX1 3PB, UK
[4]ECMWF, Robert-Schuman-Platz 3, 53175 Bonn, Germany

Correspondence: Jake P. Keller (j.p.keller@pgr.reading.ac.uk)

Abstract. High-impact weather occurring during periods of low forecast skill can lead to severe socio-economic consequences. This study examines the predictability of the causal chain of events leading to the formation of Medicane Daniel and its associated flooding impacts over Greece on 5 September and Northeast Libya on 10-11 September 2023. Daniel's formation was preceded by Hurricane Franklin's extratropical transition over the North Atlantic on 1 September 2023, the development of an Omega-type block over central Europe on 3 September 2023, and the detachment of a PV streamer over the eastern Mediterranean which led to Daniel's formation as a cut-off low on 5 September 2023. Using a novel block error metric, we investigate the predictability of these events using operational ECMWF and Met Office ensemble forecasts and ERA5 reanalysis.

Ensemble sensitivity analysis identifies Franklin's location as a leading source of downstream uncertainty. Accurate prediction of Franklin's track was critical for developing an upper-level ridge and European blocking. In ensemble members that best represented the European block, Franklin remained anchored to a downstream ridge, excited a Rossby wave packet over Europe, and initiated a wave breaking event that produced the cut-off leading to the development of Storm Daniel. Two distinct high error recurvature scenarios are identified across the forecasting systems, both of which lead to poor representation of blocking and subsequently to no Mediterranean cyclone development. The strength of Franklin's interaction with the midlatitude flow, and therefore the downstream impact of extratropical transition, is highly sensitive to small track errors at short forecast lead times. Together, these results demonstrate how small upstream errors can contribute to poor predictability of high-impact weather, reinforcing the need for improved representation of the physical processes that take place during tropical–extratropical interactions in operational forecasting to better protect vulnerable regions from impactful weather events.

1 Introduction

In early September 2023, a period of high-impact weather (HIW) affected Europe and the Mediterranean. A Mediterranean cyclone, Storm Daniel, formed near Greece on 5 September bringing persistent heavy rainfall and severe flooding to Greece and

https://doi.org/10.5194/egusphere-2026-4273
Preprint. Discussion started: 31 July 2026

Bulgaria (Hewson et al., 2024; Flaounas et al., 2025). Daniel then meandered south and east towards Libya whilst intensifying and developing a characteristic medicane structure (Hewson et al., 2024) before making landfall, leading to further intense rainfall and catastrophic flooding in Derna. Daniel's development was preceded by a Rossby wave-breaking (RWB) event over Europe, which from 5 September onwards led to a persistent Omega blocking pattern over Central Europe, with Daniel on its eastern flank. The development of storm Daniel, together with the Omega block to the west, was associated with a period of substantially reduced forecast skill in ECMWF ensemble forecasts (Hewson et al., 2024; Flaounas et al., 2025).

Further upstream and preceding the development of the blocking pattern, Hurricane Franklin started developing from a monsoon trough over the tropical Atlantic as early as 17 August, being declared a hurricane at 1200 UTC 26 August (Beven, 2024). Franklin underwent extratropical transition (ET) in the North Atlantic at around 1800 UTC 1 September as it recurved into the midlatitudes (Beven, 2024), providing a potential source of dynamical influence on the downstream flow over Europe. ECMWF forecasts initialized before Franklin's ET exhibited substantial uncertainty over Europe, highlighting the challenges of forecasting a case of low predictability (Hewson et al., 2024). This case presents an opportunity to investigate how uncertainties associated with a recurving tropical cyclone propagate downstream and influence the development of blocking and HIW over Europe.

Tropical cyclones (TCs) often recurve into the midlatitudes and interact strongly with the large-scale flow, leading to significant downstream impacts (Reimer et al., 2008; Anwender et al., 2010; Archambault et al., 2013, 2015; Grams and Blumer, 2015). Despite substantial case-to-case and basin variability of extratropical transitions (ET) (Keller et al., 2019), many such systems evolve from warm-core TCs into cold-core, asymmetric cyclones that develop frontal structures and may persist or re-intensify (Klein et al., 2000; Grams and Archambault, 2016). These interactions are also a major source of uncertainty in numerical weather prediction (NWP) over the midlatitudes (Keller et al., 2019; Grams and Blumer, 2015; Harr and Archambault, 2016; Quinting and Jones, 2016), mainly due to the highly non-linear interaction between the TC and the midlatitude flow (Ritchie and Elsberry, 2007). In particular, the phasing between the TC and an upstream trough determines whether the interaction leads to reintensification or decay, thus shaping downstream impact pathways (Ritchie and Elsberry, 2007; Grams et al., 2013a; Keller et al., 2014). This phasing depends on the depth of the trough and its relative position to the TC (Riemer and Jones, 2010), while unfavorable configurations, such as a trough located north-east of the TC, can inhibit reintensification and prevent strong midlatitude impacts (Harr et al., 2000; Grams et al., 2013b). Error in the representation of this phasing, particularly cyclone track during ET, can therefore strongly impact predicted interaction strength and downstream flow evolution (Ritchie and Elsberry, 2007; Torn and Hakim, 2009; Grams et al., 2013a).

Transitioning TCs transport warm, moist air polewards and so often exhibit strong heating rates (Grams et al., 2011; Archambault et al., 2015). Diabatic processes play a central role in jet streak formation, downstream ridge amplification, and Rossby wave evolution during ET (Archambault et al., 2015; Grams and Blumer, 2015). The advection of upper-level negative PV anomalies, generated and maintained by latent heating near developing warm fronts or remanent TC convection, can promote ridge amplification (Quinting and Jones, 2016; Grams and Archambault, 2016) and accelerate jet streaks (Grams and Archambault, 2016). Strong divergent outflow and sustained convection during ET can further anchor and amplify the downstream ridge, exciting pre-existing Rossby wave packets (RWPs) (Archambault et al., 2015; Keller et al., 2019), while

https://doi.org/10.5194/egusphere-2026-4273
Preprint. Discussion started: 31 July 2026

latent heating leading to low-PV injection into the upper troposphere contribute to ridge amplification and block development (Steinfeld and Pfahl, 2019). However, the representation of these diabatic processes is highly sensitive to model parametrization schemes, which control the magnitude and location of latent heating maxima and divergent outflow (Joos and Forbes, 2016). The representation of latent heating depends strongly on model physics choices (Joos and Forbes, 2016; Maddison et al., 2020), introducing substantial uncertainty in the location and intensity of maximum diabatic heating. Such processes are well known to affect downstream forecast skill, including in warm conveyor belts (Joos and Wernli, 2012; Oertel et al., 2019) and mesoscale convective systems (Rodwell et al., 2013; Clarke et al., 2019; Lojko et al., 2022). Previous studies have shown that moist processes during ET can significantly amplify downstream forecast errors, highlighting the importance of diabatic heating in downstream predictability (Reimer et al., 2008; Grams and Blumer, 2015; Grams and Archambault, 2016).

Although the effects of recurving TCs in the midlatitudes have been studied extensively over the last two decades, most research has been focused on TCs in the West Pacific and consequent impacts on the midlatitude flow over the U.S. (Keller et al., 2019). Few systematic studies of North Atlantic ETs and their downstream impacts have been conducted, limiting understanding of their typical influence on downstream flow variability and predictability over Europe. Of these studies, notable cases are outlined here. Hurricane Hannah recurved into the North Atlantic during September 2008 and resulted in poor downstream predictability over Europe. Hannah developed into a mature extratropical cyclone and was associated with the elongation of a downstream PV streamer and subsequent cut-off low over the Mediterranean leading to the genesis of a Mediterranean cyclone (Grams et al., 2011). They conclude that diabatic production of PV impacted downstream ridging and positioning of HIW over Europe. Hurricane Katia, underwent ET in the North Atlantic during September 2011 and developed into a mature extratropical cyclone, leading to upper-level ridge building and the formation of a downstream PV streamer that resulted in severe convective storms over Europe (Grams and Blumer, 2015). In model simulations with Katia removed through PV inversion, no trough filamentation is observed and therefore no HIW, attributing ET to downstream impact (Grams and Blumer, 2015; Keller et al., 2019). These cases highlight the importance of ET and the potential impacts of recurving tropical on forecast skill and HIW over Europe.

Other impactful TC transition events have been studied, with Grams et al. (2011) and Keller et al. (2014) concluding that Pacific ET cases are a cause of RWP excitations and ridging over western North America, leading to cold air outbreaks on the eastern side of the block. Hoskins and Berrisford (1988) indicate that ET of Hurricane Floyd influenced the downstream development of a devastating extratropical cyclone that impacted Southern England. These studies, in conjunction with the few case studies of recurving North-Atlantic TCs mentioned prior (Grams et al., 2011; Grams and Blumer, 2015) highlight the importance of understanding the impacts of such events. Climatological studies have been unable to clearly attribute RWB to ET in the North Atlantic, as the shorter, weaker Atlantic jet is inherently more prone to RWB than its North Pacific counterpart (Keller et al., 2019). Further, Grams and Archambault (2016) note that much of the research in the field has sought to observe and understand the dynamics of ET and downstream ridge building. They outline the need for systematic investigation of the link between HIW and an upstream cyclone that undergoes ET, and acknowledge that very few studies have been able to attribute HIW to ET (Grams and Blumer, 2015).

https://doi.org/10.5194/egusphere-2026-4273
Preprint. Discussion started: 31 July 2026

In this study, we investigate how uncertainty associated with the ET of Hurricane Franklin influences the predictability of downstream blocking and HIW over Europe. this case provides a valuable test case in which small upstream uncertainties may propagate through the large-scale flow and strongly affect downstream evolution, including the development of the high-impact Mediterranean cyclone Daniel. Using ECMWF and Met Office global operational forecasts, we examine how variability in Franklin's recurvature and ET modifies forecast skill across the North Atlantic–European sector. The central questions addressed in this study are: (i) how uncertainties in the representation of Franklin's ET influence the development of large-scale blocking, and (ii) how these uncertainties propagate downstream and affect the forecast skill of HIW over Europe and the Mediterranean.

The paper is structured as follows. Section 2 provides a synoptic overview of the event. Section 3 describes the data and methodologies used, including the predictability diagnostics and sensitivity framework. Section 4 presents the results, including analyses of predictability, ensemble sensitivity, and Franklin's evolution during transition. Finally, Sections 5 and 6 discuss the implications of the results and summarise the main conclusions.

2 Synpotic Overview

At 0000 UTC 1 September 2023, TC Franklin is situated in the West Atlantic with a central pressure of 975 hPa (Beven, 2024), to the south of a strong jet streak associated with a trough near Newfoundland (Figure 1a) with a weak, meandering jet structure evident over Europe. Franklin underwent an extratropical transition (ET) at 1800 UTC 1 September 2023 (Beven, 2024) and then deepened slightly (-3 hPa through the 2 September). By 0000 UTC on 3 September (Figure 1b), Franklin had moved north-eastward and was located in the mid-Atlantic, south of a strengthened jet streak. A cut-off low formed near Iberia, south of an intensifying ridge, immediately downstream of Franklin.

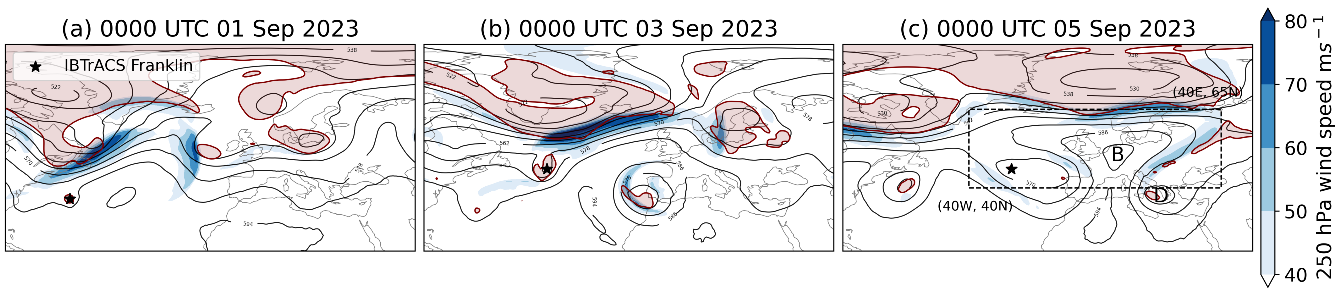

Figure 1. Synoptic evolution at 0000 UTC on 1 (a), 3 (b) and 5 (c) September 2023: 500hPa geopotential height (grey contours), the potential vorticity on the 320K surface (red contour at 2PVU and red shading > 2PVU) and 250 hPa wind speed (blue shading). Annotations the position of Franklin (star), the Omega Block (B) and Storm Daniel (D). Data from ERA5.

By 0000 UTC 5 September (Figure 1c), Franklin had weakened and moved south-eastward, merging with the cut-off low near Iberia and an Omega block (labelled B in Figure 1c) developed over Central Europe. East of the block, an arm of the jet plunged southwards across eastern Europe, associated with a filamented PV streamer evident in the 2PVU contour (Figure 1c). A trough

https://doi.org/10.5194/egusphere-2026-4273
Preprint. Discussion started: 31 July 2026

over the eastern Mediterranean deepened significantly and was coupled with a surface cyclone, which caused extensive flooding in the region and was named Storm Daniel (labelled D in Figure 1c) later that day.

This detached upper-level PV anomaly remained stationary in the Eastern Mediterranean and was unusually far south for such a feature. In ECMWF ensemble forecasts, an extreme rainfall event for Greece was detected by an increasing number of members in forecasts initialized between 30 August and 1 September (Flaounas et al., 2025). The predictability of Daniel's initial development was poor for lead times greater than 96 h (forecast initialized before 0000 UTC on September 1) (Flaounas et al., 2025), consistent with the predictability characteristics of Mediterranean cyclones (Muzio et al., 2019). Hurricane Franklin interacted with the waveguide on 1 September, and given that only the ECMWF forecasts initialized from 1 September onwards accurately predicted block onset (Hewson et al., 2024), we hypothesise that this was likely a barrier to predictability of block amplitude in the Eastern Mediterranean.

3 Data and Methods

3.1 Data

To evaluate the model forecasts we use the fifth-generation European Re-Analysis (ERA5) Hersbach et al. 2020. The data is available on a horizontal grid of approximately $0.25°$ resolution. ERA5 is used as a reference dataset for evaluating forecast behaviour and associated large-scale structures. We regrid ERA5 data to $(0.5°)$ resolution and use this as a reference to assess the predictability of the Omega block and Storm Daniel.

Ensemble forecast data from the ECMWF Ensemble Prediction System (EPS) and the global ensemble from the Met Office Global and Regional Ensemble Prediction System (MOGREPS-G) are obtained from the TIGGE archive (Swinbank et al., 2016). The ECMWF EPS consists of 51 members and has a 9km horizontal resolution and 137 vertical levels, consistent with the Cycle 48r1 physics configuration, including 4D-Var and singular vector ensemble perturbation schemes operational from June 2023 (Hewson et al., 2024). MOGREPS-G consists of 18 members and has a N640 horizontal resolution ($\approx$ 20km) and 70 vertical levels, with and physics schemes from the GA/L7.0 configuration (Walters et al., 2019) including 4D-Var and stochastic physics perturbations (Inverarity et al., 2023; Sanchez et al., 2016). Data retrieved from the TIGGE archive has $0.5°$ resolution. For this case study, daily forecasts initialized at 0000 UTC of 500 hPa geopotential height (Z500) and potential vorticity on the 320 K isentropic surface (PV320) are used. PV320 is also analysed alongside the 2 PVU contour to represent the dynamical tropopause. Additional TIGGE variables used include mean sea-level pressure (MSLP), total precipitation, and horizontal wind components at 200–300 hPa, analysed for individual ensemble members over the same period.

Track data for Hurricane Franklin are taken from the International Best Track Archive for Climate Stewardship (IBTrACS) project (Knapp et al., 2010), which provides cyclone tracks at 3-hourly intervals, including both the tropical and extratropical phases. These post-event best track data are reconstructed using all available observations, and include information on storm position, intensity (minimum pressure and maximum wind speed), and storm type. IBTrACS combines contributions from forecasting centres in each ocean basin. For North Atlantic storms such as Franklin, the National Hurricane Center provides the best track data (Knapp et al., 2010).

https://doi.org/10.5194/egusphere-2026-4273
Preprint. Discussion started: 31 July 2026

3.2 Methods

3.2.1 Block Detection

The blocking index used to identify atmospheric blocks follows the methodology of Suitters et al. (2023). Unlike traditional absolute field reversal techniques (Woollings et al., 2018), this index is based on anomalies, defining blocked grid points as large positive Z500 deviations from the zonal mean. The monthly mean climatology is removed to account for the influence of stationary Rossby wave patterns, which are especially prevalent during boreal winter (Suitters et al., 2023). Unlike many other detection methods, this Z500 anomaly–based approach imposes no persistence requirement (Woollings et al., 2018), allowing instantaneous Z500 errors to be quantified at the time of block onset, despite the block itself being a persistent feature. Z500 anomalies are defined as

$$Z_*^{'}(\lambda,\phi,t) = Z_*(\lambda,\phi,t) - \overline{Z}_*(\lambda,\phi), \tag{1}$$

where $Z_*(\lambda,\phi,t)$ is the instantaneous Z500 anomaly from the instantaneous zonal mean, and $\overline{Z}_*(\lambda,\phi)$ is the climatological monthly anomaly (1979-2021) from the climatological monthly zonal mean Z500, where a 3-month smoothing has been applied to each month's anomaly field. This climatology has been constructed by Suitters et al. (2023) using ERA5 data from 1979-2021. For this case study, an instantaneous blocked grid point is defined where $Z_*^{'} > 100$ m. This is sufficiently large to avoid detection of weaker, transient anomalies and retain only points associated with the target block.

3.2.2 Block Error Metrics

The $ZALO$ error metric, an extension of work by Suitters (2024) and is similar to SAL derived by Wernli et al. (2008) for use in forecast verification of precipitation, and PAL derived by Madonna et al. (2015) for use in forecast verification of PV anomalies in warm conveyor belt outflow and is defined as

$$ZALO = \sqrt{Z^2 + A^2 + L^2 + O^2}. \tag{2}$$

$ZALO$ is initially used to quantify the accuracy of block intensity (Z), area (A), location (L) and shape (O) in ensemble members. Z quantifies the normalised, instantaneous intensity error in the sum of $Z_*^{'}$ over a block area in an ensemble member compared to the sum of $Z_*^{'}$ over the block area in reanalysis such that,

$$Z_{fct} = \frac{\sum^{A} Z^{'}_{*fct}(t) - \sum^{A} Z^{'}_{*analysis}(t)}{\sum^{A} Z^{'}_{*fct}(t) + \sum^{A} Z^{'}_{*analysis}(t)}. \tag{3}$$

Similarly, A is the error in the block area, normalized by the sum of the blocked area in an ensemble member and the reanalysis. A can exceed one as blocks in ensemble members can be larger than in reanalysis, though is restricted within a sub-domain spanning 40W to 40E and 40N to 65N (shown in Figure 1c), centred around the Omega block over Central Europe.

https://doi.org/10.5194/egusphere-2026-4273
Preprint. Discussion started: 31 July 2026

L represents the great circle distance between the centres of mass of the blocked region in a given ensemble member, and that of the block in the reanalysis, normalized by the great circle distance of the diagonal of the region in which we look for blocked grid points, shown in Figure 1c. O is defined as $1 - O_f$, where O_f is the fraction of the block area in the analysis that is overlapped by a block in a given ensemble member. O is a novel addition to the metric, used to detect blocks in the ensemble with shapes similar to those in reanalysis. This is important as the shape of the block is linked to the amplitude of the wave-breaking event and therefore the position of the cut-off associated with Daniel. Large O implies high error, in alignment with the other block error metrics. A $ZALO$ of zero therefore represents a block that matches exactly the reanalysis in all four of these characteristic error terms within the domain of interest.

3.2.3 Tracking Franklin

A cyclone tracking algorithm was applied to the MSLP field to track Franklin's centre across successive time steps in ensemble members and in reanalysis. For each member, the zonal MSLP anomaly was calculated. The resulting anomaly field highlights synoptic-scale minima associated with cyclones. A light Gaussian smoothing of the anomaly field is applied and the cyclone centre is found as local minima within a $4° \times 4°$ spatial search window centred on the previous cyclone position, thereby enforcing temporal continuity. To improve robustness, candidate cyclone centre locations were evaluated by finding points that minimise the following parameters: MSLP anomaly, great circle distance between the new position and previous position, and local curvature of the MSLP field, estimated using the discretised second derivative of the pressure field to favour well-defined lows. The optimal cyclone position was selected within a cluster of candidate points surrounding the anomaly minimum. This approach provides a dynamically consistent estimate of the position of the cyclone while reducing sensitivity to noise, frontal structures, and competing pressure features.

3.2.4 Ensemble Sensitivity Analysis

The method used to calculate the upstream sensitivity is analogous to the methods used by Maddison et al. (2019). Here, J denotes the response function ($ZALO$) which is calculated for the 50 perturbed members of the ECMWF EPS and 17 perturbed members of MOGREPS-G. For all forecasts used, the time for which J is calculated is kept constant at 0000 UTC 5 September 2023, when the developing block becomes an established feature over Central and Northern Europe (defined as block onset) and the PV streamer develops over Eastern Europe. The sensitivity (S) at each grid point is calculated as

$$S = m \times \sigma_x \times \alpha, \tag{4}$$

where m approximates the slope coefficient as

$$m = \frac{cov(x,J)}{var(x)} = \left(\frac{\delta J}{\delta X}\right), \tag{5}$$

https://doi.org/10.5194/egusphere-2026-4273
Preprint. Discussion started: 31 July 2026

and $x = X - \overline{x}$ is the difference between the precursor field (X) and the ensemble mean ($\overline{x}$) at each grid point, and σ_x is the standard deviation of the precursor field at each grid point. α acts as a correction factor, filtering out sensitivity at grid points with weaker correlations (assuming linearity between the precursor and response function) and is defined as

$$\begin{cases} \alpha = 1, & \text{if } r^2 \geq r^2_{min}, \\ \alpha = \frac{r^2}{r^2_{min}}, & \text{if } r^2 < r^2_{min} \end{cases} \tag{6}$$

where r^2 is the coefficient of determination of the linear regression and r^2_{min} is the minimum value for which the raw sensitivity is retained at each grid point. For this case study, r^2_{min} is chosen to be 0.15 to retain only reliable sensitivities, as has been used in sensitivity studies of the midlatitudes (Maddison et al., 2019). In this case, the sensitivities have the same units as the response function and can be interpreted as the change in response function due to a one standard deviation change in the precursor field. The multiplication of sensitivity by the standard deviation of the precursor field accounts for the change in variance of the ensemble with latitude, preventing misleading sensitivity signals at latitudes where the variance is small.

4 Results

4.1 Predictability of Wave Breaking over Europe

This section examines the predictability of block onset prior to the formation of Storm Daniel. Based on preliminary predicability analyses by Hewson et al. (2024) and Flaounas et al. (2025), we hypothesize that the onset of the block was poorly forecast, as was the development of the streamer associated with Storm Daniel, since both features are manifestations of the same Rossby wave-breaking (RWB) event. We assess the predictability of these systems using block error metrics, ensemble spread and ensemble-mean error.

4.1.1 Quantifying Predictability of Omega Block Onset

Figure 2 shows the evolution of $ZALO$ and each of its components at the time of the block onset (0000 UTC 5 September 2023) with decreasing lead time. The error in block intensity, Z, varies the least with decreasing lead time (Figure 2a), with the ECMWF EPS and MOGREPS-G under and over predicting block intensity at long lead times, a desired characteristic of the ensemble systems (Figure 2b). Block area, A, is under predicted at lead times greater than 120 h by almost all members across both forecasting systems. Block location error, L, is generally small but decreases substantially between lead times of 168 and 120 h (Figure 2c). For O (Figure 2d) the lead times with the maximum error convergence rate are clear with a sharp decrease in error between the lead times of 144 and 96 h, indicative of members predicting blocking within the blocked region identified in ERA5 between these forecasts. In the combined $ZALO$ metric (Figure 2e), the best and worst blocks are effectively separated. At lead times greater than 144 h, error and spread is large across all metrics indicative of little or no skill in the prediction of block onset. Between 144 and 120 h lead times, mean error drops significantly, indicative of a predictability barrier (consistent with findings from Flaounas et al. (2025)), before slowly converging as lead time decreases.

https://doi.org/10.5194/egusphere-2026-4273
Preprint. Discussion started: 31 July 2026

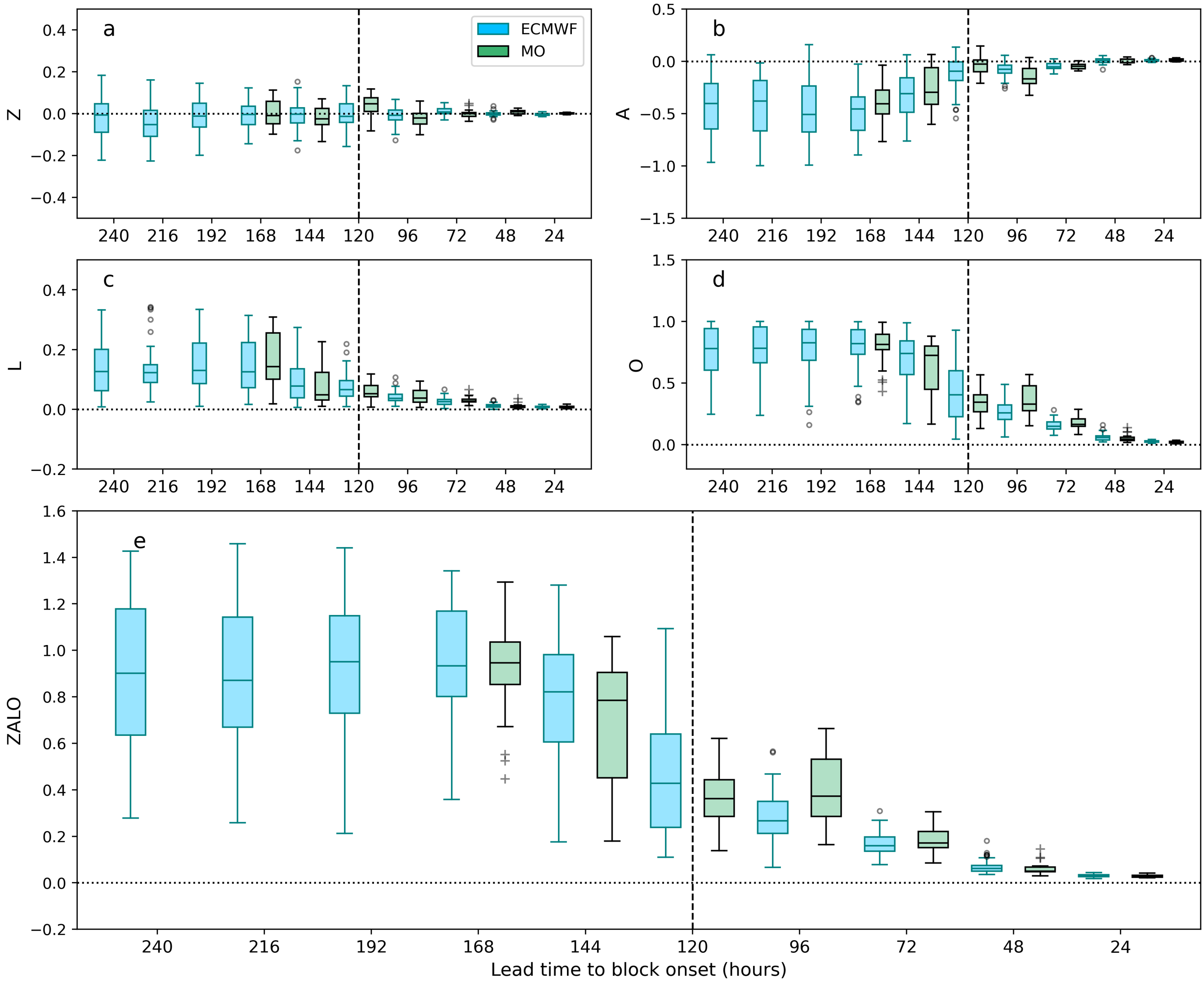

Figure 2. Block error metrics as a function of lead time to block onset (0000 UTC 5 September 2023) for both the ECMWF EPS (green) and MOGREPS-G (blue). At long lead times, ensemble members with no blocks within the detection region have been removed. Boxes denote the inter-quartile range (IQR), whiskers show $Q1 - 1.5 \times IQR$ and $Q3 + 1.5 \times IQR$ and flier points lie outside of the whiskers. The vertical, dashed line at T+120 h denotes the forecast chosen as the focus of the paper.

Although block error convergence rates in the ECMWF and Met Office ensembles are broadly similar at most lead times, there are some distinct differences. At 120 h, the Met Office ensemble performs slightly better than the ECMWF across all error metrics, exhibiting both reduced spread and lower ensemble mean error. Conversely, at 96 h the ECMWF performs better, with

https://doi.org/10.5194/egusphere-2026-4273
Preprint. Discussion started: 31 July 2026

smaller spread and lower ensemble mean error than in the Met Office forecast. The differences between forecasting systems is especially evident in the combined metric, $ZALO$ in Figure 2e.

All error metrics show the most rapid error convergence between lead times of 144 and 96 h, corresponding to forecasts initialized at 0000 UTC on 30 August and 1 September, respectively. The remainder of this section therefore focuses on the forecasts initialized at 0000 UTC on 31 August to ascertain the cause of increased forecast skill, denoted by the vertical line in Figure 2. To understand the $ZALO$ error and the development of the Omega block, the Hovmoller of spread and mean error of Z500 for the 0000 UTC cycle on 31 August (T+120 in Figure 2) are shown in Figure 3 for the latitude band of 45-55 N. In Figure 3, Franklin's position coincides with a region of high ensemble spread on 2 September in both forecasting systems, starting at 50 W as Franklin enters the latitude band. Through time, Franklin moves eastward, with an increase in forward speed occurring on 1 September (at the time of ET). The ensemble longitudes of Franklin are also shown in Figure 3 and highlight significant uncertainty in the east-west position of Franklin. In the ECMWF forecast, most ensemble members position Franklin too far to the west, with only a small number of ensemble members predicting an increase in eastward propagation of the cyclone as is seen in IBTrACS. In the Met Office forecast, a larger proportion of members position Franklin close to IBTrACS at short lead times, with the analysis lying well within the ensemble on the 3 September. A systematic and known slow TC propagation bias is observed in the ECMWF EPS (Magnusson et al., 2021), a characteristic not seen in MOGREPS-G.

Looking downstream, a region of enhanced ensemble spread in Z500 emerges in both the ECMWF and Met Office forecasts on 4 September, centred along 20E (Figure 3a,c). This region of high spread persists during and after block onset and is associated with an under-prediction of Z500 by the ensemble mean (Figure 3b,d). Comparing the ensemble mean position of the Z500 maximum in this forecast to that in ERA5, members in both forecasting systems tend to position the block centre too far to the west, with significant uncertainty regarding its eastward extent.

These features indicate substantial uncertainty in the timing of block onset and the intensity of the developing block on 5 September (at a lead time of 120 h). From the 5 September, near 50°E, both forecasts exhibit a region of positive ensemble mean error and increased ensemble spread, consistent with downstream error propagation. This behaviour is likely associated with uncertainty in the amplitude and position of the European block and the downstream cut-off low associated with Storm Daniel.

Figure 4 is the same as Figure 3 but for the latitude band 35-45 N which covers Franklin, the cut-off low over Iberia, the southernmost part of the block and, notably, Storm Daniel. In both ECMWF and Met Office forecasts, the uncertainty associated with Franklin's position is observed. The uncertainty associated with the retrogression of the cut-off low near Iberia can be seen in a tongue of increased ensemble spread, starting on 2 September and moving westward (Figure 4a,c). Ensemble spread and the under-prediction of block intensity by the ensemble mean are reduced in this latitude band, indicative of block onset being more certain, but uncertainty in its northward extent and its shape remain, as seen in the higher latitude band.

Ensemble spread and mean error associated with Storm Daniel are observed in both forecasting systems. Figure 4a,c show that a region of high spread exists around 20E, close to the ensemble mean position of Storm Daniel. The ensembles were not predicting a low as deep or as far west as is observed in reanalysis, also shown by an over-prediction of Z500 by the ensemble

https://doi.org/10.5194/egusphere-2026-4273
Preprint. Discussion started: 31 July 2026

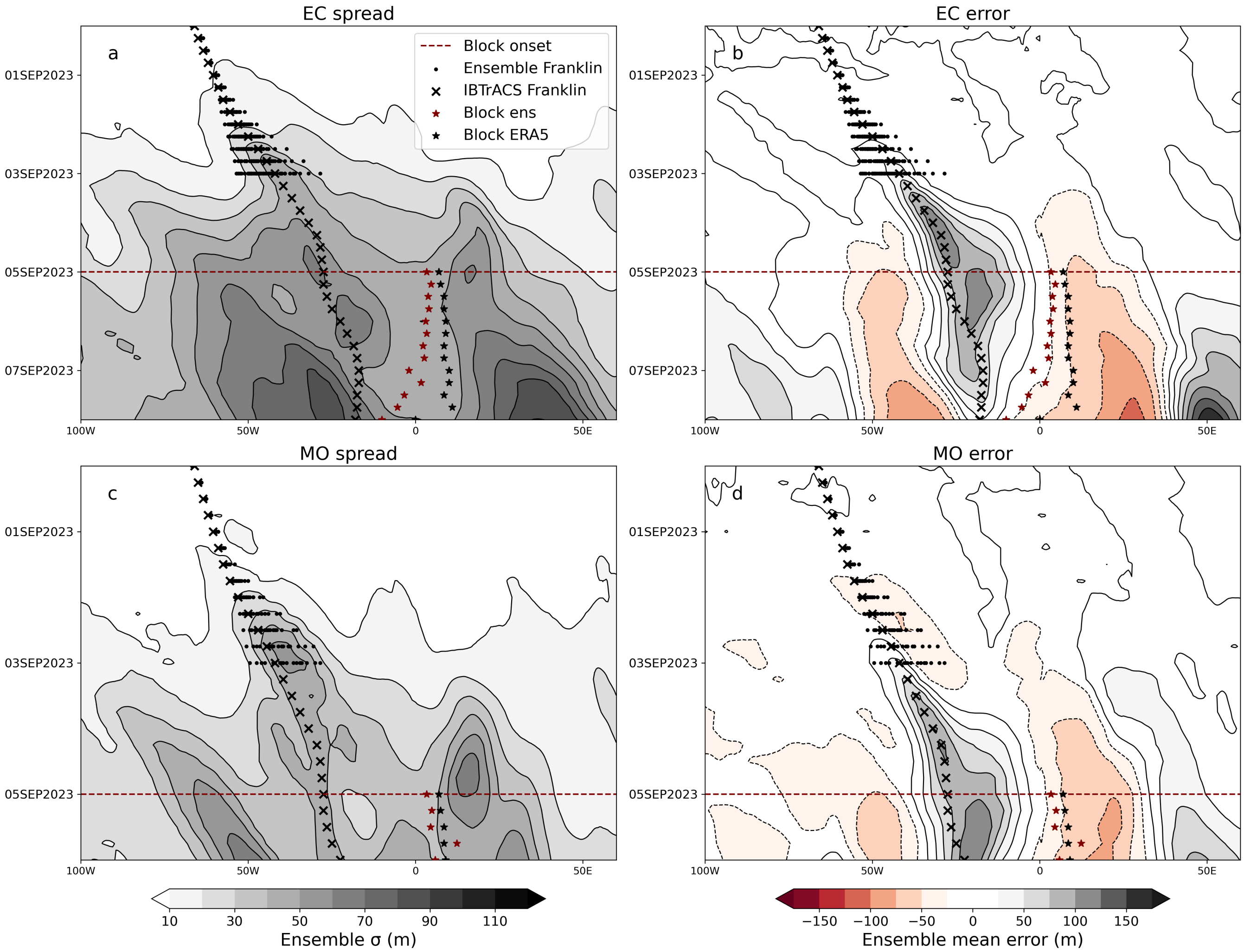

Figure 3. Hovmoller-type diagrams of ensemble standard deviation of Z500 (a,c) and ensemble mean error (b,d) in metres for ECMWF EPS (top) and MOGREPS-G (bottom) forecasts initialized at 0000 UTC 31 August 2023, averaged over the 45-55 N latitude band. The IBTrACS position of Franklin (crosses) and its position identified in each ensemble member using MSLP (dots) are shown. The ensemble mean position of the block (black stars) and its position in ERA5 (red stars) are also shown, defined here as the location of the Z500 maxima.

mean near the ERA5 position of Storm Daniel (Figure 4b,d). Errors in the eastward position of the block and westward extent to Storm Daniel occur simultaneously, indicative of the dependence of Daniel's depth and position on block amplitude, with both systems part of an amplified Rossby wave. This is increasingly evident in alternating sign of the ensemble mean error in Z500 (Figure 4b,d), demonstrating that the ensemble did not predict the amplification of the wave-like pattern associated with the stationary Omega block observed in the reanalysis.

https://doi.org/10.5194/egusphere-2026-4273
Preprint. Discussion started: 31 July 2026

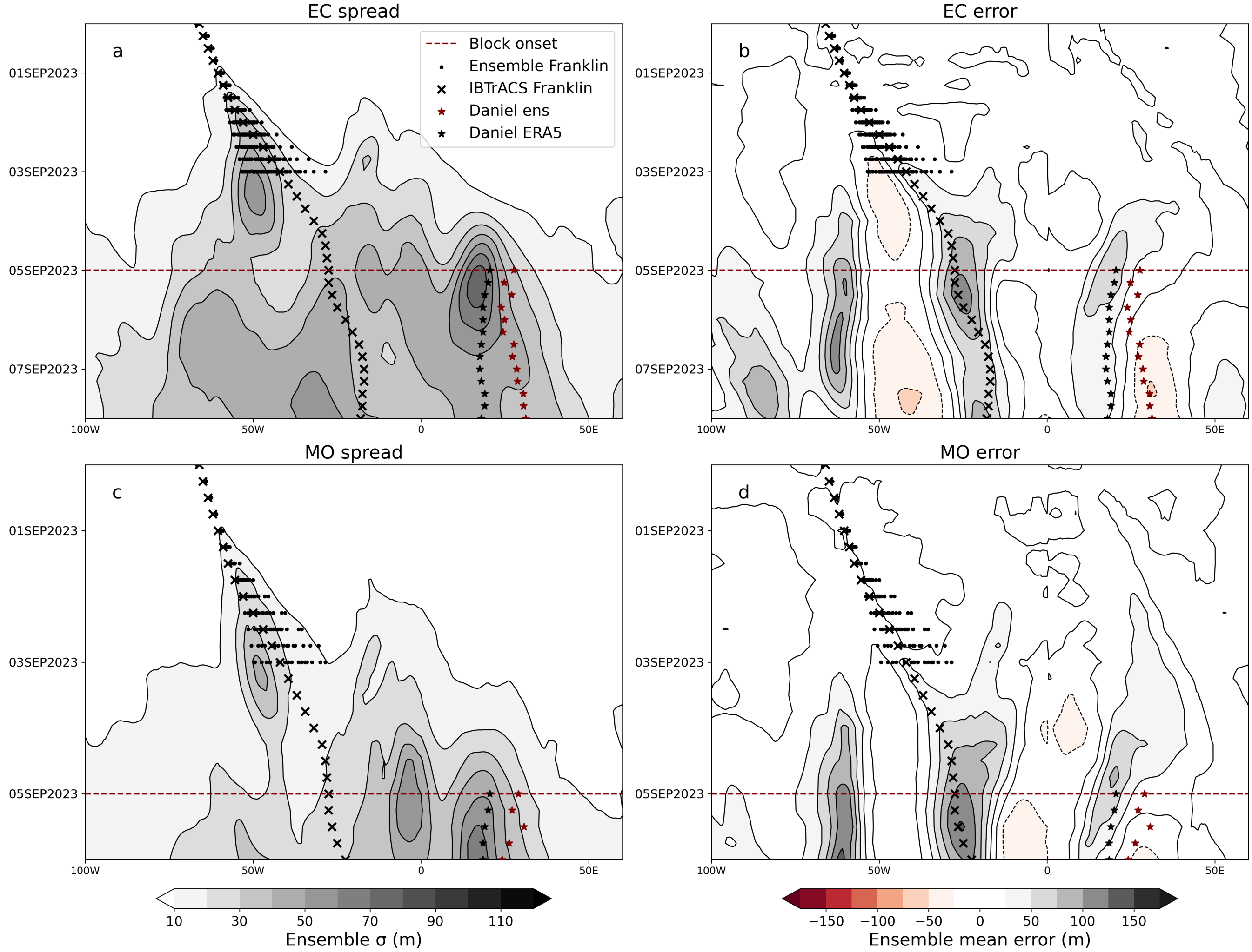

Figure 4. The same as Figure 3 but averaging over a latitude band of 35-45 N. The ensemble mean position and ERA5 position of the MSLP minima associated with storm Daniel (stars) are shown for reference.

4.2 Sensitivity Analysis

275 The influence of Franklin on European block onset and the subsequent development of Storm Daniel is examined using ensemble sensitivity analysis. We compute the sensitivity of block error ($ZALO$) to Z500 and PV320 in the days preceding block onset, focusing on ECMWF and Met Office forecasts initialized at 0000 UTC on 31 August and choose precursor fields valid at 0000 UTC on 2 and 3 September 2023. This framework allows us to follow the synoptic evolution of Franklin and downstream

https://doi.org/10.5194/egusphere-2026-4273
Preprint. Discussion started: 31 July 2026

ridge building immediately after Franklin's ET in the best and worst ensemble members. We assess how Franklin's interaction with midlatitude flow and subsequent downstream ridge development links to uncertainty in Omega block onset over Europe (discussed in Section 4.1) and observe the sensitivity of European blocking to these upstream processes.

4.2.1 Sensitivity to Z500

The sensitivity of block error ($ZALO$) at 0000 UTC 5 September 2023 to Z500 at earlier times in the forecasts initialized at 0000 UTC 31 August is shown in Figure 5. At a lead time of 48 h in ECMWF (Figure 5a), a dipole in sensitivity surrounds Franklin's position. The sign convention is such that that low block error is present in ensemble members that have low Z500 around the positive lobe of the dipole. A region of high sensitivity is also found downstream of Franklin indicating that block development over Europe is sensitive to the amplitude of ridge-building over the North Atlantic. Block error is also weakly sensitive to a trough around the southern tip of Greenland. The positions of Franklin in the three members with the lowest $ZALO$ are close to or slightly north-east of the IBTrACS position of Franklin, with the three members that produced the largest error stalling to the south-west of IBTrACS.

At a lead time of 72 h in the same forecast (Figure 5b), a similar pattern of sensitivity is observed. At this time, the south-westward error in Franklin's position in ensembles that produce poor blocks grows, whilst ensembles that produce accurate blocks remain close to the IBTrACS position of Franklin. The best members maintain interaction with the waveguide with Franklin anchored to and moving with the intensifying downstream ridge. A stronger signal for downstream ridging is evident in the best members, not only in sensitivity but the differences between dashed (high block error) and solid (low block error) Z500 contours. A wave-like pattern is evidenced by the alternating sign of sensitivity downstream of Franklin indicative of members with small errors in Franklin's position, exciting a RWP with its effects extending north-eastward towards Scandinavia.

At a lead time of 120 h (Figure 5c), the time at which the response function is evaluated, solid contours of Z500 are indicative of a more amplified and intense European block, almost to the extent observed in reanalysis. The cut-off contributing to the development of Storm Daniel is deeper and further south and west than that in members that do not amplify blocking over Europe, as is seen in Figure 4. This suggests that in the ECMWF forecast initialized at 0000 UTC 31 August, some members correctly forecast Franklin's position at short lead times, which led to downstream ridge building and therefore an accurate representation of blocking and the potential for HIW over Europe. Members in which Franklin is impacted by a slow propagation bias, do not produce an amplified Omega blocking pattern over Europe nor a cut-off low in the eastern Mediterranean, highlighting the dependence of blocking and downstream HIW on Franklin's interaction with the waveguide.

In the Met Office forecast initialized at 0000 UTC 31 August, at a lead time of 48 h (Figure 5d), differences relative to the ECMWF are apparent. The sensitivity dipole surrounding Franklin is absent, with only a weak region of positive sensitivity slightly northeast of the IBTrACS position. No clear signal links south-westward displacement to poor blocking, consistent with the lack of members exhibiting a pronounced stall of Franklin at this lead time, as is the case in the ECMWF forecast. A weak region of negative sensitivity downstream indicates block error is sensitive to downstream ridge-building, although this signal is notably weaker than in the ECMWF, reflecting less spread in the response function, as seen in Figure 2e. Sensitivity

https://doi.org/10.5194/egusphere-2026-4273
Preprint. Discussion started: 31 July 2026

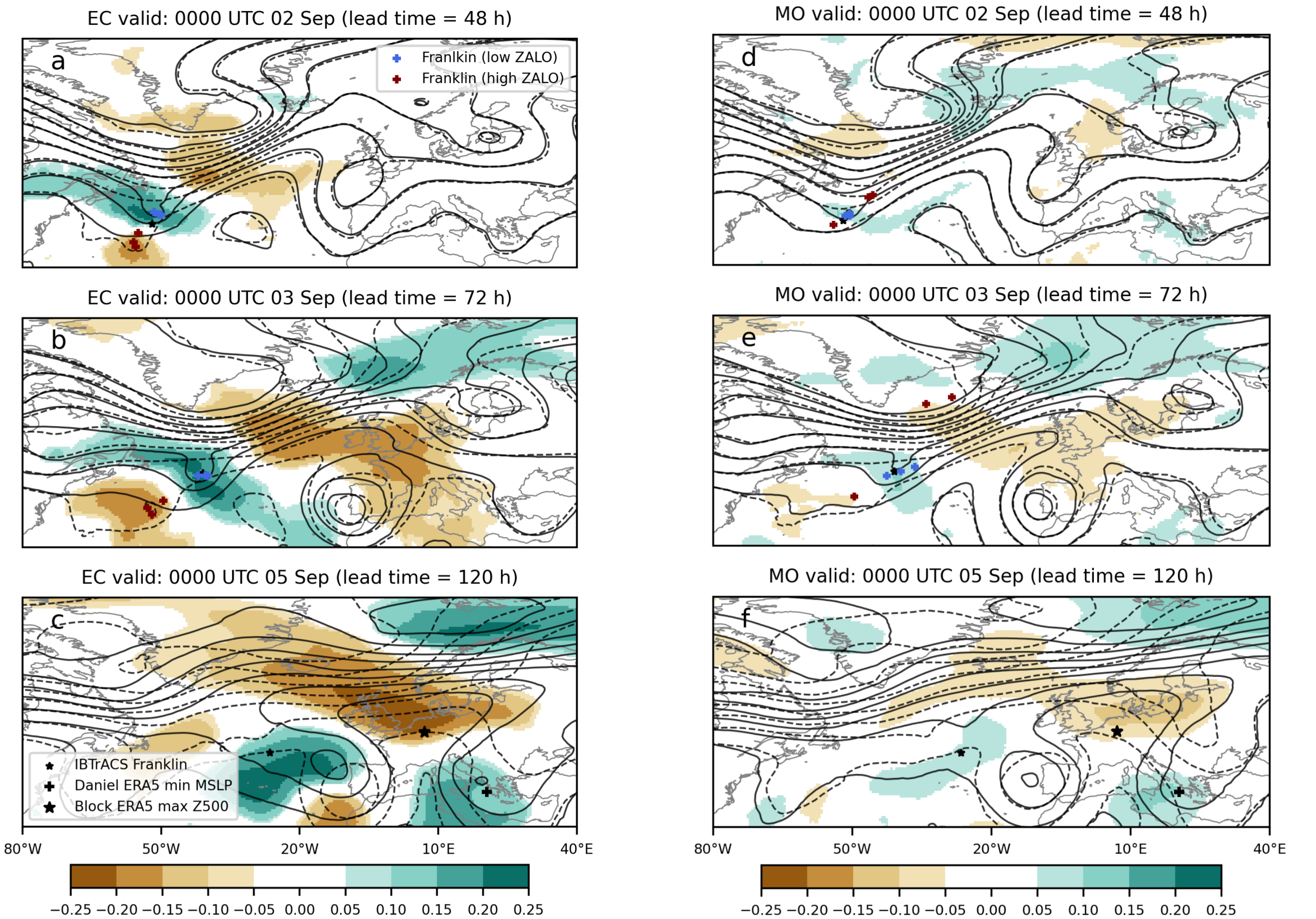

Figure 5. Sensitivity of block error ($ZALO$) at 0000 UTC 5 September 2023 sensitivity to Z500 at earlier lead times from the ECMWF (left) and Met Office (right) forecasts initialized at 0000 UTC 31 August 2023 and valid for 0000 UTC 2 September 2023 (a, d), 0000 UTC 3 September 2023 (b, e) and 0000 UTC 5 September 2023 (c, f). Contours show the mean Z500 field from the three ensemble members with the highest (dashed) and lowest (solid) $ZALO$ values. The position of Franklin in IBTrACS is shown (star) as well as its position in the three ensemble members with the highest (red dots) and lowest (blue dots) $ZALO$ values.

over the North Atlantic and south of Greenland highlights block sensitivity to an upstream short-wave trough ejected from Canada, with lower block error associated with higher Z500 and thus a weaker short-wave trough.

At a lead time of 72 h (Figure 5e), a pattern of sensitivity similar to that observed in the ECMWF at the same lead time is evident, with ensembles that produce low block error positioning Franklin close to IBTrACS. RWP excitation, like in the ECMWF, is seen in the alternating sign of sensitivity, and in the differences between solid and dashed contours a long way downstream of Franklin.

https://doi.org/10.5194/egusphere-2026-4273
Preprint. Discussion started: 31 July 2026

At a lead time of 120 h (Figure 5f), the best members capture the position of the block and its north-eastward extent, with a defined trough associated with Daniel developing in the correct location. Poor members do not have an amplified block and, though they do develop a trough downstream of the ridge, lack the development of a highly filamented trough that extends into the Eastern Mediterranean.

In general, the sensitivity magnitudes in the Met Office forecast are weaker than in the ECMWF, reflecting both reduced spread in the response function ($ZALO$; Figure 2) and the presence of multiple pathways to poor blocking. These include both a slight south-westward displacement and rapid north-eastward recurvature of Franklin, which reduces covariance between precursor fields and the response function and limit the assumption of linearity. Linearity is restored when removing the two rapidly recurving members resulting in slightly stronger sensitivities (not shown), though covariance is still weakened by reduced spread in $ZALO$. Despite these differences, a consistent signal emerges across forecasting systems. Accurate blocking is associated with Franklin tracking close to IBTrACS, the development of downstream ridging at short lead times, and the excitation of a RWP. In contrast, poor members fail to sustain ridge amplification and downstream wave development, even when interaction with the midlatitude flow is strong. Thus, recurvature scenarios are distinguished not only by Franklin's position, but by the extent and persistence of its dynamical coupling to the waveguide.

4.2.2 Sensitivity to PV320

Block development over Europe is sensitive to the position of Franklin and Rossby wave amplification. However, to observe the impact of this positional uncertainty on the waveguide, ensemble sensitivity is calculated with PV320 as the precursor field. Figure 6 shows the ensemble sensitivity of $ZALO$ to PV320 for the same ECMWF and Met Office forecasts at the same lead times as in Figure 5. Focusing first on the ECMWF forecast, at a lead time of 48 h (Figure 6a), a weak dipole in sensitivity develops, centred near the position of Franklin in IBTrACS, similar to the patterns observed in the Z500. The impact of small track differences on the waveguide is already evident, with separation of the low error and high error 2PVU contours to the north and east of Franklin.

At a lead time of 72 h (Figure 6b), a defined dipole of sensitivity develops around Franklin. Significant upper-level ridge building is evident in members with low block error, a feature not observed in the poorest members in which Franklin has stalled significantly south-west of IBTrACS. Between the 2PVU contours of the mean PV320 field of the high and low error member groups is a region of strong, positive sensitivity, suggesting low block error is associated with significant upper-level ridge building and thus low PV in this region. Downstream of the ridge, the eastern portion of the trough extends eastward, with negative sensitivities encompassed by the 2PVU contours of the high and low error ensemble groups. At a lead time of 120 h (Figure 6c), the three ensembles with the lowest block error, the 2PVU line sits further north over Europe and a highly filamented PV streamer extends further south than those with the highest block error, with a segmented streamer becoming cut off near the ERA5 position of Storm Daniel.

As is the case in Z500 sensitivity, ensemble sensitivity in the Met Office forecast initialized at 0000 UTC 31 August, shows a different picture to its ECMWF counterpart. At a 48 h lead time (Figure 6b), two poor block-producing members that recurve quickly north-eastward are clearly visible as a region of high PV enclosed within the dashed red contour to the north-east

https://doi.org/10.5194/egusphere-2026-4273
Preprint. Discussion started: 31 July 2026

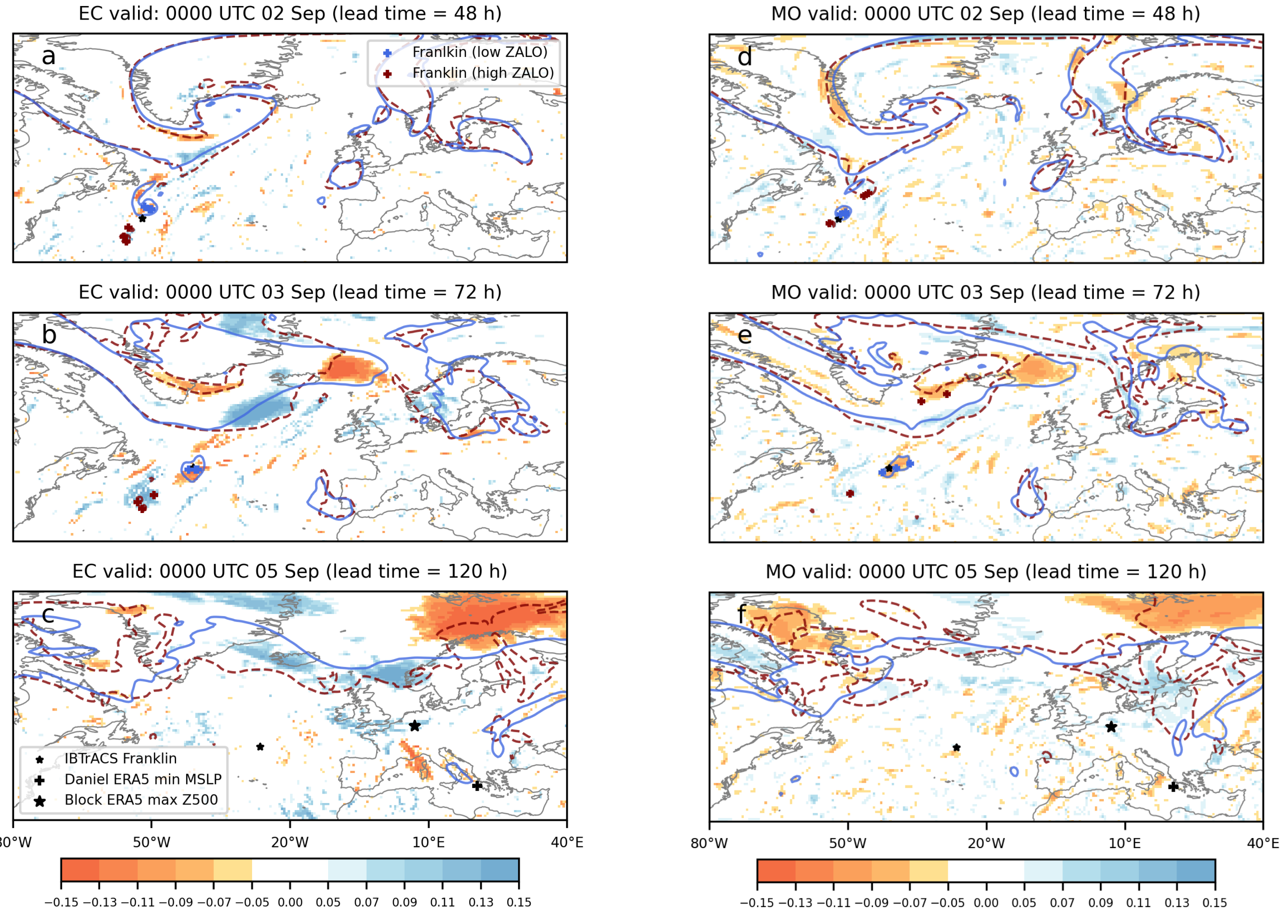

Figure 6. The same as Figure 5 but showing $ZALO$ sensitivity to PV320 at the same lead times. Contours show the 2PVU line of the mean field from the three ensemble members with highest (pink dashed) and lowest (purple) $ZALO$.

of Franklin's IBTrACS position. There is a region of positive sensitivity associated with these members, confirming that the cyclonic PV tower associated with Franklin in this region is synonymous with high block error. Members that produce accurate blocks are situated near to the IBTrACS position and are visible in the closed, blue 2PVU contour.

At a 72 h lead time (Figure 6e), the 2PVU contour of the low block error members (blue) shows ridge building south of Iceland, but not to the extent observed in the corresponding ECMWF forecast. Differences between the red dashed and blue contours are less pronounced than in the ECMWF, in part because the best MOGREPS-G members produce slightly less ridging, but also because poorest members are split over two recurvature scenarios that produce more upper-level ridging than the poorest ECMWF members. A region of sensitivity between these contours is indicative of block error sensitivity to this upper-level ridge building. At 120 h (Figure 6f), members that produce accurate blocks also produce a PV streamer over eastern Europe. Members with high block error produce a broader trough with no evidence of wave-breaking. This is similar to

https://doi.org/10.5194/egusphere-2026-4273
Preprint. Discussion started: 31 July 2026

patterns observed in the ECMWF forecast, indicating the block and streamer are part of the same RWB which is only accurately represented when Franklin's position at short lead times is correct, allowing for sustained upper level ridging as the cyclone undergoes ET.

The position of Franklin is significant when ensuring low downstream error in the Omega block pattern over Europe. Both the ECMWF and Met Office ensembles indicate that accurate blocks are produced when Franklin is close to the IBTrACS position, resulting in sustained mid- and upper-level ridge building indicative of phasing between Franklin and the midlatitude flow. In members where Franklin stalls to the south-west of the IBTrACS position of Franklin, interaction with the midlatitude flow is limited, and there is little or no upper-level ridge building. This results in poor blocking and poor representation of the location and depth of the cut-off associated with Storm Daniel.

In the Met Office ensembles, poor blocks are achieved by ensembles that stall and interact less with the midlatitude flow, or interact heavily with the upstream trough and recurve north-eastwards quickly at short lead times. These ensembles fail to phase lock with the upstream trough and subsequently, the downstream, upper-level ridge development at short lead times is not anchored to Franklin and does not become an amplified feature over Europe. A lack of coupling between the TC and downstream ridge has been observed in weak TC-waveguide interactions, such as that of Typhoon Jangmi Grams et al. (2013b), where small changes in Jamgmi's starting position had a significant impact on the downstream flow. Across both forecasting systems, three distinct and physically plausible recurvature scenarios lead to contrasting interactions with the waveguide and downstream impacts.

4.2.3 Forecast Error in Individual Ensemble Members

Although forecast uncertainty and error over Europe and the North Atlantic have so far been assessed from an ensemble perspective, further insight into recurvature scenarios identified through sensitivity analysis can be gained by investigating Franklin's representation during ET in individual ensemble members.

Figure 7 shows the latitude and longitude error in Franklin's position in the ensemble members for the ECMWF and Met Office ensembles at 48 and 72 h lead times for the forecasts initialized at 0000 UTC 31 August. Block accuracy is highly dependent on Franklin's position in the ECMWF forecast at a 48 h lead time, with accurate blocks produced by members that position Franklin slightly north-east of IBTrACS. At a 72 h lead time (Figure 7b) members that produce poor good blocks follow IBTrACS almost exactly, with members that produce poor blocks positioning Franklin to the south and west of Franklin's true position, with clear clusters of high and low block error members evident, explaining the strong observed sensitivity signal. The members that produce the largest block error exhibit the slow propagation bias observed in Figure 3 and Figure 4.

In the Met Office forecast initialized on 31 August, similarly to the ECMWF, members that produce good blocks position Franklin close to IBTrACS at both forecast lead times. In two of the ensemble members, Franklin recurves too quickly, becoming part of a frontal wave which becomes entrenched within the trough centred around Greenland (not shown). This non-linear behaviour is absent in the ECMWF forecast and helps explain the weaker relationship between block error and Franklin's position seen in the sensitivity signal in the Met Office forecast. Of the three worst-performing Met Office members, the poorest

https://doi.org/10.5194/egusphere-2026-4273
Preprint. Discussion started: 31 July 2026

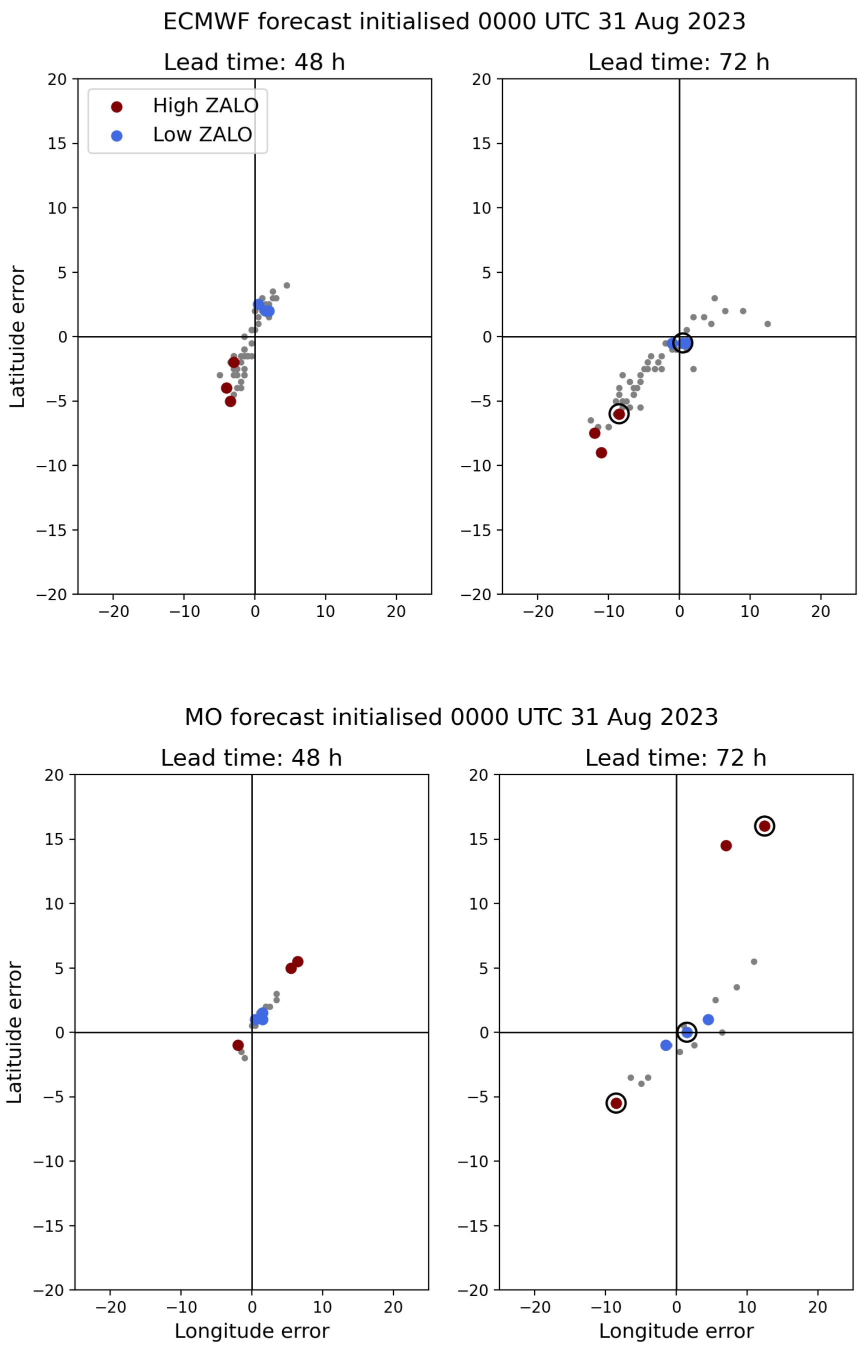

Figure 7. Franklin's position compared with IBTrACS for forecasts initialized at 0000 UTC 31 August at 48 and 72 h lead times. The ECMWF (top) and Met Office (bottom) ensembles are shown. The three highest and lowest $ZALO$ members are plotted in red and blue, respectively. Circled are the ECMWF members with the highest and lowest $ZALO$, and the two highest and one lowest $ZALO$ Met Office members at 72 h.

https://doi.org/10.5194/egusphere-2026-4273
Preprint. Discussion started: 31 July 2026

member stalls south and west of IBTrACS with the second poorest recurving quickly northwards (circled in Figure 7). Three distinct recurvature scenarios are evident, with the best block-producing members positioning Franklin close to IBTrACS and bookended by very different recurvature scenarios in the forecasts initialized at 0000 UTC 31 August across both forecasting systems.

4.3 Franklin During Transition

At short forecast lead times, Franklin's position influences its interaction with the waveguide and, consequently, the maintenance of downstream ridge building during ET. However, to understand why differences in Franklin's interactions with the waveguide lead to contrasting downstream outcomes in the three recurvature extremes identified, we observe how Franklin interacts with the jet at the time of ET.

Here, Franklin's characteristics at the time of ET are examined for the best and poorest members from the ECMWF forecast (circled in Figure 7), focusing on how Franklin evolves in response to its interaction with the jet streak in these two recurvature extremes (Figure 8). There are marked differences in the distribution and intensity of precipitation between these members, with the low error ensemble developing a region of intense precipitation at 0000 UTC 2 September. This intense precipitation persists before Franklin develops frontal features as it moves north-eastward. Franklin follows the jet entrance region of the jet streak, which maintains its strong and coherent structure. The member with the highest error has precipitation much further to the south, and a sudden enhancement of organised precipitation at 0000 UTC 2 September is not observed. Franklin is unable to follow the eastward propagating jet streak, which then weakens through the 2 September, limiting coupling between these systems. The best ECMWF ensemble member places Franklin slightly further north by 1200 UTC 1 September, enabling it to move in phase with the jet and maintain prolonged interaction with the waveguide, thereby sustaining the upper-level forcing needed for intense, persistent precipitation and resultant outflow.

In the Met Office forecast initialized on 31 August, three physically plausible scenarios are observed. Of these three, two distinct recurvature scenarios were identified that lead to poor blocking, with one leading to accurate blocking (circled in Figure 7). Figure 9 is the same as Figure 8 but shows the best and the poorest two members from the Met Office forecast. The best MOGREPS-G member (labelled low $ZALO$) behaves similarly to the best ECMWF member, remaining close to the jet streak with organised and intense precipitation developing by 0000 UTC 2 September. Franklin's close proximity to the strong jet streak persists until 1200 UTC 2 September as Franklin develops frontal features.

In the poorest member (labelled High $ZALO$ 1), enhanced precipitation and a slight deepening is observed, but occurs much later than in the best member, around 1200 UTC 2 September. Franklin is also much further south at all lead times, meaning any outflow from Franklin is not allowed to interact significantly with the jet region. In the second poorest member, which recurved very quickly north-eastward (labelled High $ZALO$ 2), enhanced precipitation associated with Franklin is already established at 1200 UTC 1 September, a scenario not observed in the ECMWF. Franklin is then steered towards and into the jet streak, which weakens as the circulation associated with Franklin disrupts the jet-level flow.

In this forecast, clear differences emerge in how Franklin influences the jet between well-performing and poorly-performing members. In the best members, a strong jet streak is maintained, whereas in poorly performing Met Office members the jet

https://doi.org/10.5194/egusphere-2026-4273
Preprint. Discussion started: 31 July 2026

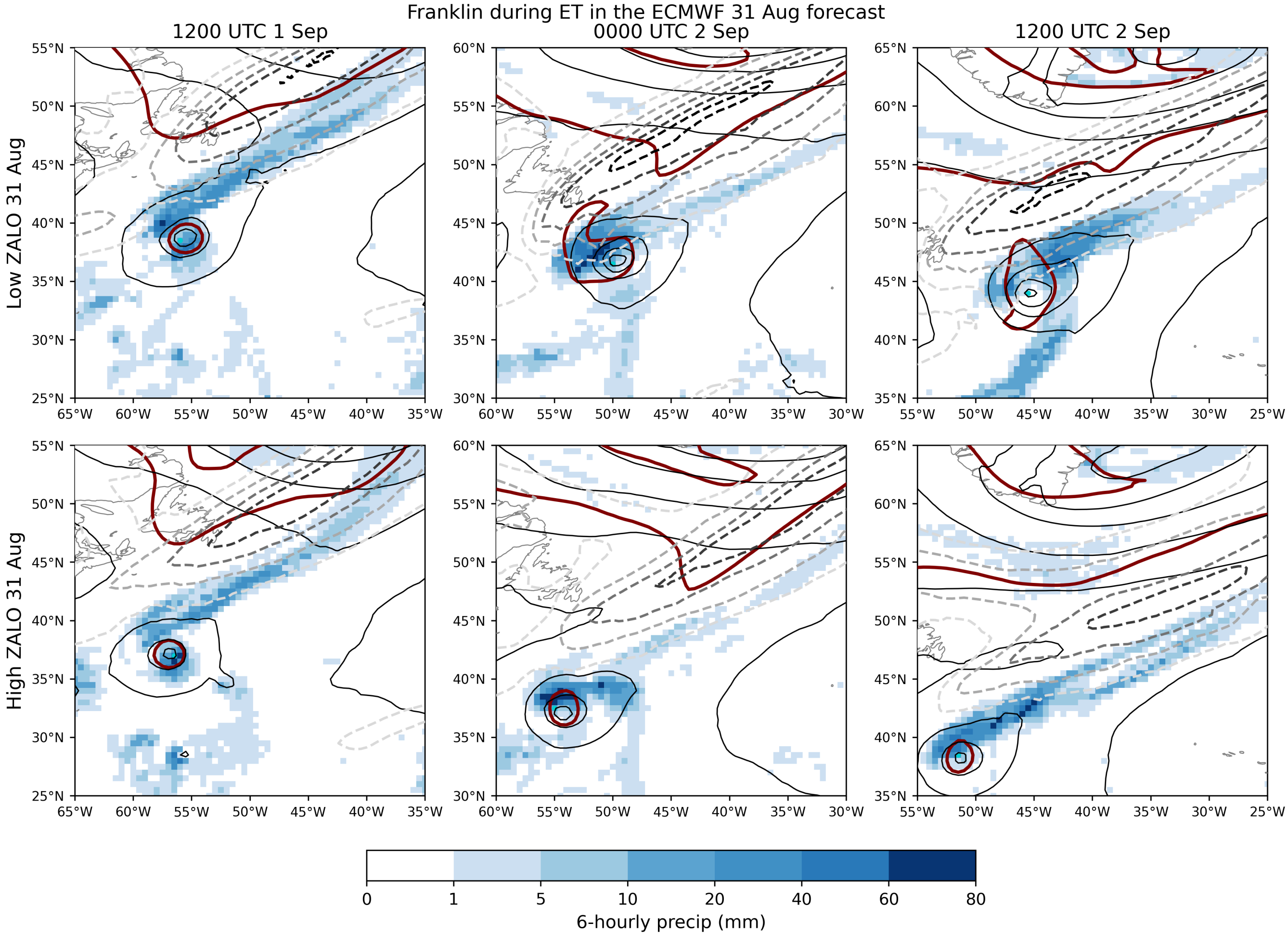

Figure 8. Mean 6-hourly total precipitation (blue shading), jet level (200-300 hPa) winds (dashed contours), and the 2PVU contour of the ensemble member with the highest and the lowest $ZALO$ for the ECMWF forecast initialized at 1200 UTC 1 September, 0000 UTC 2 September and 1200 UTC 2 September.

weakens substantially and the jet streak structure is modified by Franklin's circulation and its interaction with the waveguide. Although these poorer Met Office members do exhibit enhanced precipitation, the timing of this enhancement and its position relative to the jet are critical in determining the accuracy of the downstream block. The underlying cause of these contrasting results can be traced back to small TC track errors with very short lead times. This highlights the importance of the representation of phasing between the transitioning TC and the upstream trough, consistent with the framework proposed by (Klein et al., 2002; Reimer et al., 2008), in which the timing of latent heat release and its anchoring to the downstream ridge play a key role in shaping downstream flow evolution.

https://doi.org/10.5194/egusphere-2026-4273
Preprint. Discussion started: 31 July 2026

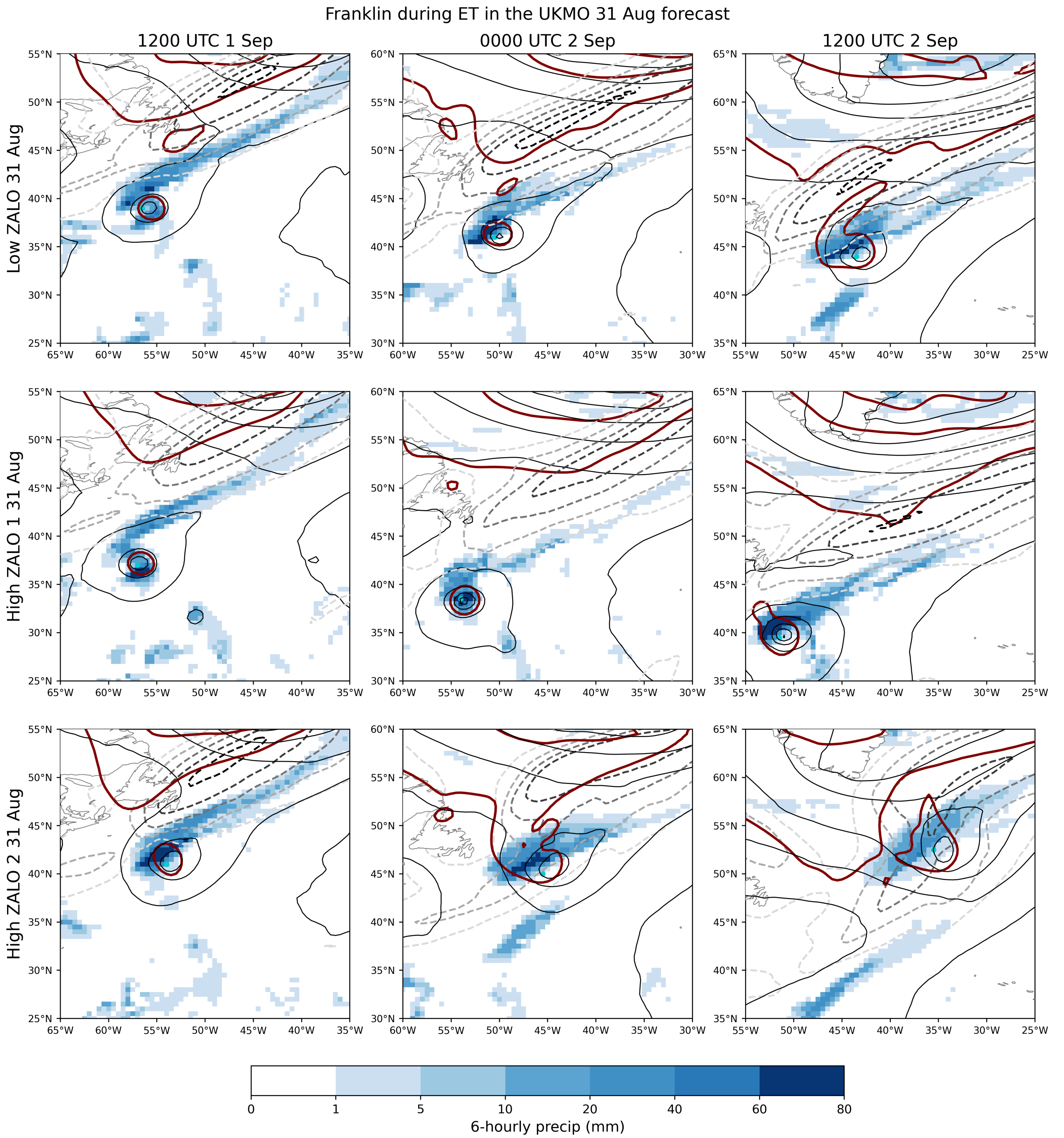

Figure 9. Mean 6-hourly total precipitation (blue shading), jet level (200-300 hPa) winds (dashed contours), and the 2PVU contour of the ensemble member with the highest $ZALO$ and the two members with the lowest $ZALO$, illustrating the three recurvature scenarios in the Met Office forecast initialized at 0000 UTC 31 August.

https://doi.org/10.5194/egusphere-2026-4273
Preprint. Discussion started: 31 July 2026

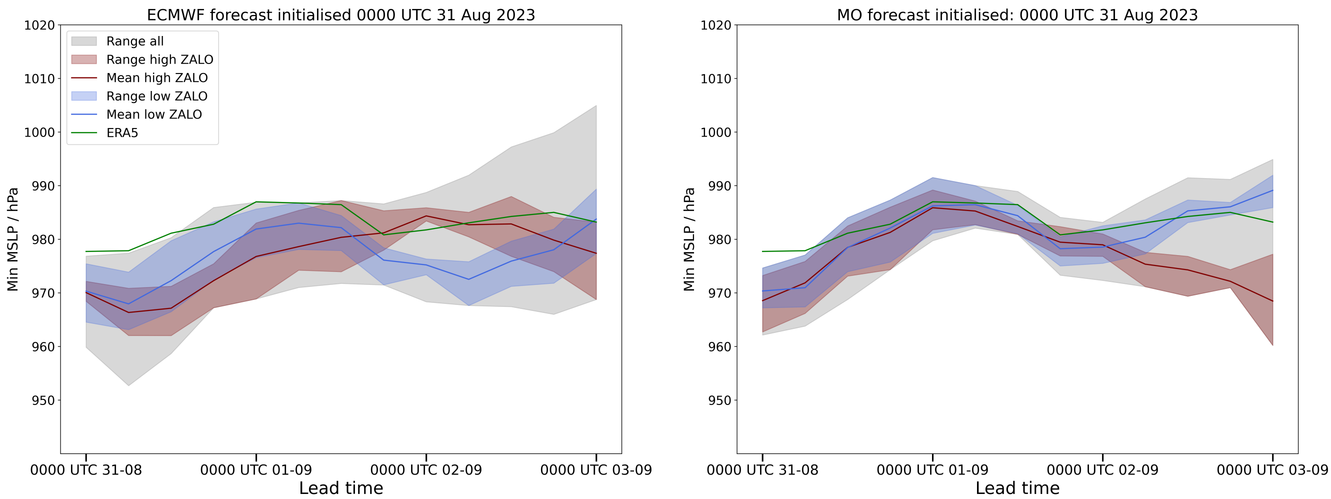

Figure 10. Ensemble fan plots of Franklin's minimum MSLP for the first 72 h of ECMWF EPS forecasts (left) and Met Office ensemble forecasts (right) initialized at 0000 UTC 31 August. The groups of three ensembles with the highest and lowest $ZALO$ in each forecast are plotted in red and blue respectively.

Figure 10 shows how Franklin's minimum MSLP changes through the first 72 h of the ECMWF and Met Office forecasts initialized 31 August. In the ECMWF forecast initialized on 31 August, the best members undergo significant deepening in MSLP as precipitation intensifies, and follow similar patterns of re-intensification to Franklin in ERA5. Franklin in poorest members continues to weaken as good ensembles intensify. In the Met Office forecast initialized on 31 August, the best members follow a very similar pattern to their ECMWF counterparts with significant deepening evident from 1200 UTC 1 September followed by weakening from 1800 UTC 1 September. However, in the Met Office, the poorest members also undergo re-intensification at the same time as the best members. This is likely due to the fact that poor block-producing ensembles in this Met Office forecast include two ensembles that recurve quickly north-eastwards and therefore also re-intensify at the same time as the best members. The member in this subset that stalled south-west of IBTrCAS also undergoes re-intensification, though with a delayed increase in precipitation (Figure 9). It should be noted that Franklin's initial MSLP and MSLP at the time of midlatitude flow interaction is similar between the best and worst members, indicative of position being the key driver of downstream uncertainty as opposed to TC intensity.

Although both good and poor member groups undergo re-intensification, they produce markedly different blocking scenarios. This indicates that Franklin's position relative to the jet during re-intensification, along with the location and strength of its outflow, strongly influences downstream evolution, including blocking and the development of the cut-off low associated with Storm Daniel. Although an unfavourable northeast–southwest orientation limits the extent of re-intensification, it is the phasing with the jet, associated diabatic processes and sustained ridge building that have the greatest influence on downstream blocking and HIW.

https://doi.org/10.5194/egusphere-2026-4273
Preprint. Discussion started: 31 July 2026

5 Discussion

This case demonstrates that small differences in Franklin's development at short lead times place the cyclone one of three physically plausible recurvature scenarios, resulting in substantially different downstream outcomes in terms of blocking and Mediterranean cyclone development. The best performing members in this case study exhibit sustained downstream ridge building and jet streak maintenance. This allows for a brief period of phase locking between the developing ridge and the transitioning TC. This is coherent with findings from Quinting and Jones (2016) and Archambault et al. (2015), where climatologically, ETs that have the most impact on the midlatitude flow were found to phase lock and anchor with the downstream ridge. This also corroborates the research by Harr et al. (2000); Ritchie and Elsberry (2007) and Grams et al. (2013b), who found that TC-trough interactions have been shown to be highly dependent on small track errors and the characteristics of the midlatitude flow pattern into which the TC moves.

A study of Typhoon Jangmi by Grams et al. (2013b) highlights the dependence of TC interaction and subsequent downstream impact on small track difference. They find that longitudinal track changes of Jangmi on the order of just 1.25 degrees (128 km) result in contrasting downstream scenarios, and an eastward shift of just 2.5 degrees can be attributed to reintensification and RWP excitation. The same was found to be true if Jamngmi is shifted northward by the same distance. Contrasting downstream flow evolution in members that place Franklin in slightly different positions (Figure 7) is similar to behaviour seen in the case of Jamgmi, with just a few degrees separating Franklin in the best and poorest performing members at short forecast lead times. When Franklin's position follows the IBTrACS, Franklin's speed of propagation increases, allowing Franklin to follow jet streak and to re-intensify. Prolonged interaction with the waveguide allows for strong and persistent downstream ridge amplification. In ECMWF members with a slow propagation bias, Franklin stalls at a bifurcation point (as in the case of Jamgmi) and therefore do not interact with the waveguide. Met Office members that propagate too quickly at short lead times quickly recurve and re-intensify but do not achieve phase locking, leading to a lack of sustained ridge amplification.

Sensitivity of blocking to a short-wave trough ejected from Canada in the ECMWF and Met Office forecasts indicates that this feature may have influenced Franklin's position early in the forecast, causing a cascade of error growth downstream. Given the complexity of interaction between systems steering Franklin during recurvature, more work is required to determine cause of these errors. With downstream uncertainty dependant on Franklin at such short lead times, forecast skill is likely highly dependant on initial condition perturbation schemes, which vary between NWP centres. More work is required to ascertain the impact of ensemble perturbation schemes on forecast skill in ET cases, though prior studies (Komaromi et al., 2011) along with previously discussed sensitivity experiments (Grams et al., 2013b) demonstrate that the outcome of ET is greatly influenced by initial condition perturbations.

The sensitivity of a recurving TC to a midlatitude trough observed here is also reflected in idealised ET frameworks. Harr et al. (2000) determined that re-intensification and coupling with the midlatitude flow to a cyclone undergoing ET is prevented for 36 h when the trough is to the north-east of the cyclone. However, here coupling and re-intensification of Franklin in the best performing ensembles occurs immediately after ET, with the trough axis to the north-east of Franklin. Harr et al. (2000) generalise cases based on phasing with the upstream trough, though they do highlight the case-to-case dependency of

https://doi.org/10.5194/egusphere-2026-4273
Preprint. Discussion started: 31 July 2026

interaction strength with the size of the systems themselves. Franklin is an example of this, with Franklin's recurvature likely not solely influenced by the near stationary Greenland trough but also a short-wave trough. Poor representation of these systems within the ensemble may have introduced the observed small track errors at short lead times. However, there are other factors that may explain the significant downstream impact of Franklin's ET.

The strong downstream impact of Franklin on the midlatitudes despite its unfavourable position for re-intensification with reference to the upper level trough could be attributed to its proximity to a strong jet streak, allowing re-intensification due to upper-level forcing for ascent. Archambault et al. (2015) found that the strongest interactions occur often when the TC transitions near an equator-ward jet entrance, maintaining ascent and aiding coupling between the TC and downstream ridge. Archambault et al. (2015) also indicate that the weak downstream jet structure favours high-impact anticyclonic wave-breaking, as is the case with Franklin's ET. Although the observed strength of interaction with the midlatitudes was extremely marginal in the case of Franklin, the downstream jet structure likely amplified the observed impact of ET.

In the case of Franklin, after ET and during re-intensification, an enhancement in precipitation occurs, observed in ensembles that produce accurate blocking. Re-intensification is position dependent, with members in which Franklin stalls south of the jet exhibiting a delayed re-intensification or none at all. However, when Franklin is positioned close to upper-level divergence at the jet entrance, re-intensification and enhanced precipitation is observed. Grams et al. (2011) found that the remnants of tropical, low-level PV in Ex-Hurricane Hannah enhanced poleward moisture advection and allowed for intense mid-level diabatic production of PV. The extent to which the enhancement in convection was forced by low-level warm air advection or upper-level divergence is unclear given methodologies used here, though it is plausible that in the best ensembles, both factors could have played a role in conditioning the environment for a sudden bust of convection and latent heat release that contributed to phase locking (Torn and Hakim, 2009; Archambault et al., 2015) and accurate block representation in the best members.

Poor-performing members, namely those in which Franklin recurves northward too quickly in the Met Office forecast, also experience reintensification and increased precipitation. The position of Franklin with reference to the jet and the time of convective initiation likely played a key role in Franklin's downstream impact, with only the best ensembles producing precipitation in the location and at the time observed in reanalysis and observations (not shown). This diabatic heating and reintensification, likely maintained the strength of low PV advection across the baroclinic zone, ridge building and anchoring (Figures 5 and 6), and aided jet streak intensification (Figures 8 and 9). Sustained upper-level ridge building then led to wave-breaking and the development of a cut-off, aiding the intensification of Storm Daniel. We therefore infer the role of diabatic processes on downstream predictability may be significant. However, the extent to which latent heating impacted blocking and HIW is unclear, and will be explored in later work. Together, these results highlight how marginal differences in TC evolution during ET can cascade into large downstream forecast errors, highlighting the combined roles of phasing, jet interaction, and diabatic processes in limiting midlatitude predictability.

https://doi.org/10.5194/egusphere-2026-4273
Preprint. Discussion started: 31 July 2026

6 Conclusions

The predictability of the chain of events leading up to the formation of an impactful Mediterranean cyclone, Storm Daniel, has been evaluated using an anomaly-based block detection method, a novel block error metric, and ensemble sensitivity analysis. We chose to focus on the block as an intermediary between Franklin upstream and Storm Daniel downstream. The start of this chain of events occurred when hurricane Franklin recurved into the midlatitudes and underwent ET east of Newfoundland at 1800 UTC 1 September 2023 (Beven, 2024). Ex-Franklin then pushed eastwards, deepening slightly as an extratropical system, preceded by a developing downstream ridge. As the ridge moved into western Europe, a Rossby-wave breaking event that developed as an upper-level low, already situated over eastern Europe, plunged southward, forming a PV streamer, while an Omega block became established over Europe at 0000 UTC 5 September. The detached streamer led to the formation of a cut-off low in the eastern Mediterranean and the formation of Storm Daniel, which had devastating impacts for Greece and Bulgaria and later Libya.

The predictability of block onset, at 0000 UTC 5 September 2023, was examined using the $ZALO$ error metric for ECMWF and Met Office ensemble forecasts initialized at 0000 UTC 31 August 2023. Both forecasting systems struggled to capture the onset and north-eastward extent of the Omega block. The errors in block amplitude are directly related to the lack of development of the PV streamer and the cut-off low required for the development of Storm Daniel, highlighting the coupling between the predictability of European blocking and downstream Mediterranean cyclogenesis.

Block error has been shown to be sensitive to three distinct recurvature scenarios of Franklin on days prior to block onset over Europe. These three distinct recurvature scenarios only become evident when both ECMWF and Met Office forecasts are jointly analysed. Ensemble sensitivity shows that members that position Franklin closest to the observed track (IBTrACS) at the time of midlatutude flow interaction produce the most accurate blocks, demonstrating that representation of phasing between Franklin and the midlatitude flow is crucial for ridge amplification, Rossby wave breaking, and subsequent blocking. In contrast, high-error scenarios arise when Franklin stalls at a bifurcation point, limiting interaction with the waveguide, or when it recurves rapidly northward and merges with the Greenland low. Both pathways lead to limited ridge building and poor representation of blocking. These findings are consistent with previous work (Grams et al., 2013a; Ritchie and Elsberry, 2007), demonstrating that the strength of extratropical transition depends strongly on the phasing between the tropical cyclone and midlatitude trough. Small track errors at short lead times, concurrent with Franklin's interaction with flow bifurcation, represent a key barrier to predictability of downstream wave amplification, blocking, and associated high-impact weather.

Although errors in Franklin's track are the primary driver of downstream uncertainty, the timing and location of diabatic processes relative to the waveguide may impact blocking and high-impact weather development. In members that produce accurate blocks, Franklin undergoes re-intensification near the equatorward jet entrance, accompanied by enhanced convective precipitation, consistent with cases in previous studies (Harr et al., 2000; Grams et al., 2011; Keller et al., 2019). The associated latent heating likely strengthens interaction with the waveguide and promotes ridge amplification, in line with idealised and composite analyses (Archambault et al., 2015). This diabatic enhancement supports jet streak acceleration and downstream coupling, processes identified in prior ET cases (Grams and Archambault, 2016). However, while re-intensification and

https://doi.org/10.5194/egusphere-2026-4273
Preprint. Discussion started: 31 July 2026

enhanced precipitation occur across many ensemble members, only those in which it is correctly positioned relative to the large-scale flow lead to sustained dynamical coupling and accurate blocking. This highlights that diabatic effects can amplify, but not compensate for, positional errors, reinforcing their secondary but important role in shaping downstream predictability.

The role of diabatic processes therefore warrants further investigation to isolate the relative contribution of positional errors and latent heating in flow amplification during Franklin's ET. Although the results here suggest that downstream forecast error is sensitive to Franklin's track, diabatic feedbacks likely contribute to the evolution of downstream impacts over Europe. A key question for future work is whether resolving Franklin's position alone is sufficient to constrain downstream uncertainty, or whether the improved representation of diabatically driven processes during ET is also required. This research will advance our understanding of forecast skill during ET and will improve the prediction of Mediterranean cyclone cases arising from upstream, non-linear interactions.

Code and data availability. The codes used to obtain the results in this work are available from the lead author upon request. The ERA5 data used for the reanalysis can be freely obtained from the ECMWF Copernicus Climate Change Service (C3S) website (https://doi.org/10.24381/cds.143582cf). This work is based on TIGGE data. TIGGE (The International Grand Global Ensemble) is an initiative of the World Weather Research Programme (WWRP). TIGGE data is published under a Creative Commons Attribution Non-Commercial 4.0 International (CC BY NC 4.0). To view a copy of this licence, visit https://creativecommons.org/licenses/by-nc/4.0/legalcode.

Author contributions. Jake Keller: Conceptualization, Data curation, Formal analysis, Investigation, Methodology, Software, Validation, Visualization, Writing (original draft preparation), Writing (review and editing); Oscar Martínez-Alvarado: Conceptualization, Funding acquisition, Methodology, Resources, Supervision, Writing (review and editing); Ben Harvey: Conceptualization, Funding acquisition, Methodology, Resources, Supervision, Writing (review and editing); Claudio Sanchez: Conceptualization, Funding acquisition, Methodology, Resources, Supervision, Writing (review and editing); Benoit Vanniere: Conceptualization, Funding acquisition, Methodology, Supervision, Writing (review and editing)

Competing interests. The contact author has declared that none of the authors have any competing interests.

Acknowledgements. JK was supported by the University of Reading Advancing the Frontiers of Earth System Prediction (AFESP) Programme (award number A3720300). OMA and BH acknowledge funding from the NERC CANARI programme (NE/W004984/1).

https://doi.org/10.5194/egusphere-2026-4273
Preprint. Discussion started: 31 July 2026

References

Anwender, D., Jones, S. C., Leutbecher, M., and Harr, P. A.: Sensitivity experiments for ensemble forecasts of the extratropical transition of Typhoon Tokage (2004), Quarterly Journal of the Royal Meteorological Society, 136, 183–200, https://doi.org/10.1002/qj.527, 2010.

Archambault, H. M., Bosart, L. F., Keyser, D., and Cordeira, J. M.: A climatological analysis of the extratropical flow response to recurving western north pacific tropical cyclones, Monthly Weather Review, 141, 2325–2346, https://doi.org/10.1175/MWR-D-12-00257.1, 2013.

Archambault, H. M., Keyser, D., Bosart, L. F., Davis, C. A., and Cordeira, J. M.: A composite perspective of the extratropical flow response to recurving western North Pacific tropical cyclones, Monthly Weather Review, 143, 1122–1141, https://doi.org/10.1175/MWR-D-14-00270.1, 2015.

Beven, J. L.: Hurricane Franklin, Tech. Rep. AL082023, National Hurricane Center, 2024.

Clarke, S. J., Gray, S. L., and Roberts, N. M.: Downstream influence of mesoscale convective systems. Part 1: influence on forecast evolution, Quarterly Journal of the Royal Meteorological Society, 145, 2933–2952, https://doi.org/10.1002/qj.3593, 2019.

Flaounas, E., Dafis, S., Davolio, S., Faranda, D., Ferrarin, C., Hartmuth, K., Hochman, A., Koutroulis, A., Khodayar, S., Miglietta, M. M., Pantillon, F., Patlakas, P., Sprenger, M., and Thurnherr, I.: Dynamics, predictability, impacts and climate change considerations of the catastrophic Mediterranean Storm Daniel (2023), Weather and Climate Dynamics, 6, 1515–1538, https://doi.org/10.5194/wcd-6-1515-2025, 2025.

Grams, C. M. and Archambault, H. M.: The Key Role of Diabatic Outflow in Amplifying the Midlatitude Flow: A Representative Case Study of Weather Systems Surrounding Western North Pacific Extratropical Transition, Monthly Weather Review, https://doi.org/10.1175/MWR-D-15-0419.s1, 2016.

Grams, C. M. and Blumer, S. R.: European high-impact weather caused by the downstream response to the extratropical transition of North Atlantic Hurricane Katia (2011), Geophysical Research Letters, 42, 8738–8748, https://doi.org/10.1002/2015GL066253, 2015.

Grams, C. M., Wernli, H., Böttcher, M., Čampa, J., Corsmeier, U., Jones, S. C., Keller, J. H., Lenz, C. J., and Wiegand, L.: The key role of diabatic processes in modifying the upper-tropospheric wave guide: A North Atlantic case-study, Quarterly Journal of the Royal Meteorological Society, 137, 2174–2193, https://doi.org/10.1002/qj.891, 2011.

Grams, C. M., Jones, S. C., and Davis, C. A.: The impact of Typhoon Jangmi (2008) on the midlatitude flow. Part II: Downstream evolution, Quarterly Journal of the Royal Meteorological Society, 139, 2165–2180, https://doi.org/10.1002/qj.2119, 2013a.

Grams, C. M., Jones, S. C., Davis, C. A., Harr, P. A., and Weissmann, M.: The impact of Typhoon Jangmi (2008) on the midlatitude flow. Part I: Upper-level ridgebuilding and modification of the jet, Quarterly Journal of the Royal Meteorological Society, 139, 2148–2164, https://doi.org/10.1002/qj.2091, 2013b.

Harr, P. A. and Archambault, H. M.: Dynamics, predictability, and high-impact weather associated with the extratropical transition of tropical cyclones, pp. 153–167, Cambridge University Press, https://doi.org/10.1017/cbo9781107775541.013, 2016.

Harr, P. A., Elsberry, R. L., and Hogan, T. F.: Extratropical Transition of Tropical Cyclones over the Western North Pacific. Part II: The Impact of Midlatitude Circulation Characteristics, Monthly Weather Review, 2000.

Hersbach, H., Bell, B., Berrisford, P., Hirahara, S., Horányi, A., Muñoz-Sabater, J., Nicolas, J., Peubey, C., Radu, R., Schepers, D., Simmons, A., Soci, C., Abdalla, S., Abellan, X., Balsamo, G., Bechtold, P., Biavati, G., Bidlot, J., Bonavita, M., Chiara, G. D., Dahlgren, P., Dee, D., Diamantakis, M., Dragani, R., Flemming, J., Forbes, R., Fuentes, M., Geer, A., Haimberger, L., Healy, S., Hogan, R. J., Hólm, E., Janisková, M., Keeley, S., Laloyaux, P., Lopez, P., Lupu, C., Radnoti, G., de Rosnay, P., Rozum, I., Vamborg, F., Vil-

https://doi.org/10.5194/egusphere-2026-4273
Preprint. Discussion started: 31 July 2026

laume, S., and Thépaut, J. N.: The ERA5 global reanalysis, Quarterly Journal of the Royal Meteorological Society, 146, 1999–2049, https://doi.org/10.1002/qj.3803, 2020.

Hewson, T. D., Ashoor, A., Boussetta, S., Lagouvardos, K., Lavers, D., Magnusson, L., Pillosu, F., and Zsoter, E.: 81555-newsletter-no-179-spring-2024, Tech. rep., ECMWF, https://doi.org/doi:10.21957/lr71sf656j, 2024.

Hoskins, B. and Berrisford, P.: A POTENTIAL VORTICITY PERSPECTIVE OF THE STORM OF 15–16 OCTOBER 1987, Weather, 43, 122–129, https://doi.org/10.1002/j.1477-8696.1988.tb03890.x, 1988.

Inverarity, G. W., Tennant, W. J., Anton, L., Bowler, N. E., Clayton, A. M., Jardak, M., Lorenc, A. C., Rawlins, F., Thompson, S. A., Thurlow, M. S., Walters, D. N., and Wlasak, M. A.: Met Office MOGREPS-G initialisation using an ensemble of hybrid four-dimensional ensemble variational (En-4DEnVar) data assimilations, Quarterly Journal of the Royal Meteorological Society, 149, 1138–1164, https://doi.org/10.1002/qj.4431, 2023.

Joos, H. and Forbes, R. M.: Impact of different IFS microphysics on a warm conveyor belt and the downstream flow evolution, Quarterly Journal of the Royal Meteorological Society, 142, 2727–2739, https://doi.org/10.1002/qj.2863, 2016.

Joos, H. and Wernli, H.: Influence of microphysical processes on the potential vorticity development in a warm conveyor belt: A case-study with the limited-area model COSMO, Quarterly Journal of the Royal Meteorological Society, 138, 407–418, https://doi.org/10.1002/qj.934, 2012.

Keller, J. H., Jones, S. C., and Harr, P. A.: An Eddy Kinetic Energy View of Physical and Dynamical Processes in Distinct Forecast Scenarios for the Extratropical Transition of Two Tropical Cyclones*, Monthly Weather Review, https://doi.org/10.1175/MWR-D, 2014.

Keller, J. H., Grams, C. M., Riemer, M., Archambault, H. M., Bosart, L., Doyle, J. D., Evans, J. L., Galarneau, T. J., Griffin, K., Harr, P. A., Kitabatake, N., McTaggart-Cowan, R., Pantillon, F., Quinting, J. F., Reynolds, C. A., Ritchie, E. A., Torn, R. D., and Zhang, F.: The extratropical transition of tropical cyclones. Part II: Interaction with the midlatitude flow, downstream impacts, and implications for predictability, https://doi.org/10.1175/MWR-D-17-0329.1, 2019.

Klein, P. M., Harr, P. A., and Elsberry, R. L.: Extratropical Transition of Western North Pacific Tropical Cyclones: An Overview and Conceptual Model of the Transformation Stage, Monthly Weather Review, 2000.

Klein, P. M., Harr, P. A., and Elsberry, R. L.: Extratropical Transition of Western North Pacific Tropical Cyclones: Midlatitude and Tropical Cyclone Contributions to Reintensification, Monthly Weather Review, 2002.

Knapp, K. R., Kruk, M. C., Levinson, D. H., Diamond, H. J., and Neumann, C. J.: The international best track archive for climate stewardship (IBTrACS), Bulletin of the American Meteorological Society, 91, 363–376, https://doi.org/10.1175/2009BAMS2755.1, 2010.

Komaromi, W. A., Majumdar, S. J., and Rappin, E. D.: Diagnosing initial condition sensitivity of Typhoon Sinlaku (2008) and Hurricane Ike (2008), Monthly Weather Review, 139, 3224–3242, https://doi.org/10.1175/MWR-D-10-05018.1, 2011.

Lojko, A., Payne, A., and Jablonowski, C.: The Remote Role of North-American Mesoscale Convective Systems on the Forecast of a Rossby Wave Packet: A Multi-Model Ensemble Case-Study, Journal of Geophysical Research: Atmospheres, 127, https://doi.org/10.1029/2022JD037171, 2022.

Maddison, J. W., Gray, S. L., Martínez-Alvarado, O., and Williams, K. D.: Upstream cyclone influence on the predictability of block onsets over the Euro-Atlantic region, Monthly Weather Review, 147, 1277–1296, https://doi.org/10.1175/MWR-D-18-0226.1, 2019.

Maddison, J. W., Gray, S. L., Martínez-Alvarado, O., and Williams, K. D.: Impact of model upgrades on diabatic processes in extratropical cyclones and downstream forecast evolution, Quarterly Journal of the Royal Meteorological Society, 146, 1322–1350, https://doi.org/10.1002/qj.3739, 2020.

https://doi.org/10.5194/egusphere-2026-4273
Preprint. Discussion started: 31 July 2026

Madonna, E., Boettcher, M., Grams, C. M., Joos, H., Martius, O., and Wernli, H.: Verification of North Atlantic warm conveyor belt outflowsin ECMWF forecasts, Quarterly Journal of the Royal Meteorological Society, 141, 1333–1344, https://doi.org/10.1002/qj.2442, 2015.

Magnusson, L., Majumdar, S., Emerton, R., Richardson, D., Alonso-Balmaseda, M., Baugh, C., Bechtold, P., Bidlot, J., Bonanni, A., Bonavita, M., Bormann, N., Brown, A., Browne, P., Carr, H., Dahoui, M., Chiara, G. D., Diamantakis, M., Duncan, D., English, S., Forbes, R., Geer, A., Haiden, T., Healy, S., Hewson, T., Ingleby, B., Janousek, M., Kuehnlein, C., Lang, S., Lock, S.-J., Mcnally, T., Mogensen, K., Pappenberger, F., Polichtchouk, I., Prates, F., Prudhomme, C., Rabier, F., Rosnay, P. D., Quintino, T., Rennie, M., Titley, H., Vana, F., Vitart, F., Warrick, F., Wedi, N., and Zsoter, E.: Tropical cyclone activities at ECMWF, Tech. rep., ECMWF, http://www.ecmwf.int/publications/, 2021.

Muzio, E. D., Riemer, M., Fink, A. H., and Maier-Gerber, M.: Assessing the predictability of Medicanes in ECMWF ensemble forecasts using an object-based approach, Quarterly Journal of the Royal Meteorological Society, 145, 1202–1217, https://doi.org/10.1002/qj.3489, 2019.

Oertel, A., Boettcher, M., Joos, H., Sprenger, M., Konow, H., Hagen, M., and Wernli, H.: Convective activity in an extratropical cyclone and its warm conveyor belt – a case-study combining observations and a convection-permitting model simulation, Quarterly Journal of the Royal Meteorological Society, 145, 1406–1426, https://doi.org/10.1002/qj.3500, 2019.

Quinting, J. F. and Jones, S. C.: On the Impact of Tropical Cyclones on Rossby Wave Packets: A Climatological Perspective, Monthly Weather Review, https://doi.org/10.1175/MWR-D-14-00298.s1, 2016.

Reimer, M., Jones, S. C., and Davis, C. A.: The impact of extratropical transition on the downstream flow: An idealized modelling study with a straight jet, Quarterly Journal of the Royal Meteorological Society, 134, 69–91, https://doi.org/10.1002/qj.189, 2008.

Riemer, M. and Jones, S. C.: The downstream impact of tropical cyclones on a developing baroclinic wave in idealized scenarios of extratropical transition, Quarterly Journal of the Royal Meteorological Society, 136, 617–637, https://doi.org/10.1002/qj.605, 2010.

Ritchie, E. A. and Elsberry, R. L.: Simulations of the extratropical transition of tropical cyclones: Phasing between the upper-level trough and tropical cyclones, Monthly Weather Review, 135, 862–876, https://doi.org/10.1175/MWR3303.1, 2007.

Rodwell, M. J., Magnusson, L., Bauer, P., Bechtold, P., Bonavita, M., Cardinali, C., Diamantakis, M., Earnshaw, P., Garcia-Mendez, A., Isaksen, L., Källén, E., Klocke, D., Lopez, P., McNally, T., Persson, A., Prates, F., and Wedi, N.: Characteristics of occasional poor medium-range weather forecasts for Europe, Bulletin of the American Meteorological Society, 94, 1393–1405, https://doi.org/10.1175/BAMS-D-12-00099.1, 2013.

Sanchez, C., Williams, K. D., and Collins, M.: Improved stochastic physics schemes for global weather and climate models, Quarterly Journal of the Royal Meteorological Society, 142, 147–159, https://doi.org/10.1002/qj.2640, 2016.

Steinfeld, D. and Pfahl, S.: The role of latent heating in atmospheric blocking dynamics: a global climatology, Climate Dynamics, 53, 6159–6180, https://doi.org/10.1007/s00382-019-04919-6, 2019.

Suitters, C.: The Role of Anticyclonic Transient Eddies in Atmospheric Blocking Dynamics, Ph.D. thesis, University of Reading, 2024.

Suitters, C. C., Martínez-Alvarado, O., Hodges, K. I., Schiemann, R. K., and Ackerley, D.: Transient anticyclonic eddies and their relationship to atmospheric block persistence, Weather and Climate Dynamics, 4, 683–700, https://doi.org/10.5194/wcd-4-683-2023, 2023.

Swinbank, R., Kyouda, M., Buchanan, P., Froude, L., Hamill, T. M., Hewson, T. D., Keller, J. H., Matsueda, M., Methven, J., Pappenberger, F., Scheuerer, M., Titley, H. A., Wilson, L., and Yamaguchi, M.: The TIGGE project and its achievements, Bulletin of the American Meteorological Society, 97, 49–67, https://doi.org/10.1175/BAMS-D-13-00191.1, 2016.

https://doi.org/10.5194/egusphere-2026-4273
Preprint. Discussion started: 31 July 2026

Torn, R. D. and Hakim, G. J.: Initial condition sensitivity of Western Pacific extratropical transitions determined using ensemble-based sensitivity analysis, Monthly Weather Review, 137, 3388–3406, https://doi.org/10.1175/2009MWR2879.1, 2009.

Walters, D., Baran, A. J., Boutle, I., Brooks, M., Earnshaw, P., Edwards, J., Furtado, K., Hill, P., Lock, A., Manners, J., Morcrette, C., Mulcahy, J., Sanchez, C., Smith, C., Stratton, R., Tennant, W., Tomassini, L., Weverberg, K. V., Vosper, S., Willett, M., Browse, J., Bushell, A., Carslaw, K., Dalvi, M., Essery, R., Gedney, N., Hardiman, S., Johnson, B., Johnson, C., Jones, A., Jones, C., Mann, G., Milton, S., Rumbold, H., Sellar, A., Ujiie, M., Whitall, M., Williams, K., and Zerroukat, M.: The Met Office Unified Model Global Atmosphere 7.0/7.1 and JULES Global Land 7.0 configurations, Geoscientific Model Development, 12, 1909–1963, https://doi.org/10.5194/gmd-12-1909-2019, 2019.

Wernli, H., Paulat, M., Hagen, M., and Frei, C.: SAL - A novel quality measure for the verification of quantitative precipitation forecasts, Monthly Weather Review, 136, 4470–4487, https://doi.org/10.1175/2008MWR2415.1, 2008.

Woollings, T., Barriopedro, D., Methven, J., Son, S. W., Martius, O., Harvey, B., Sillmann, J., Lupo, A. R., and Seneviratne, S.: Blocking and its Response to Climate Change, https://doi.org/10.1007/s40641-018-0108-z, 2018.